

Testing of a Bridge Weigh-in-Motion Algorithm Based on Multiple Longitudinal Sections

Arturo González¹, Jason Dowling¹, Eugene J. OBrien¹, Ales Žnidarič²

¹ University College Dublin, Ireland.

² ZAG, Ljubljana, Slovenia.

Abstract

A new Bridge Weigh-in-Motion (WIM) algorithm is developed which makes use of strain sensors at multiple longitudinal locations. The optimisation procedure at the core of the proposed algorithm seeks to minimise the difference between static theory and measurement, a procedure common in the majority of Bridge WIM algorithms. In contrast to the single unique value calculated for each axle weight in common Bridge WIM algorithms, the algorithm proposed herein applies the optimisation procedure to a set of equations formulated at each scan of the Bridge WIM system, to give a time history of calculated axle weights. Studying the determinant of the system of equations devised at each scan, those portions of the time history of calculated axle weights for which the system of equations is poorly conditioned are removed from the final reckoning of the axle weights. The proposed algorithm makes use of a robust moving average filter to remove much of the effects of dynamics. A calibration procedure based on using trucks from ambient traffic and the effect of the number of calibration vehicles on accuracy are investigated. The influence of additional longitudinal sensor locations on the determinant of the system equations is also discussed. Sensitivity analyses are carried out to analyse the effect of a misread axle spacing or velocity on the predictions, and as a result, a novel addition to the proposed algorithm allows for identifying potentially erroneous predictions. The improvement in accuracy of the calculated axle weights by the proposed algorithm is shown, firstly using numerical simulations based on a vehicle-bridge interaction finite element model and secondly using experimental data from a beam-and-slab bridge in Slovenia.

1. Introduction

The weighing of vehicles in motion is a valuable source of information to local authorities and governing bodies for allocation of resources regarding infrastructure planning, traffic policing and overload enforcement in addition to the interest at a macro level, concerning economic development via trade corridors. Static weighing stations provide exact weights of axles, but interrupt the flow of traffic, introducing delays into the transportation network. There is also the tendency to obtain biased data sets due to driver knowledge of the location, and subsequent avoidance, of the weighing stations [Sivakumar et al. 2008].

There are three main systems to weigh vehicles at full highway speeds: (a) pavement-based Weigh-in-Motion (WIM) systems, (b) Bridge WIM systems, and (c) On-board Weigh-In-Motion systems, requiring instrumentation of the vehicle [Kenyon 1996]. WIM systems use weighing detectors embedded into or placed on the road surface to measure axle (or wheel) pressures. The wheels of the vehicles being weighed are typically in contact with the weighing device of a WIM system for the order of a few milliseconds [WAVE 2001]. However, this contact time is not long enough to determine the current state of bounce or hop of the axle for the time of measurement. Hence the axles are easily over- or under-weighed. Therefore, WIM systems are subject to relatively rapid degradation due to their direct exposure to environmental and traffic loads. Bridge WIM systems regard bridges as weighing scales to weigh vehicles as they traverse at full highway speeds. They are limited by the need to find a suitable bridge in the route to be monitored. On the one hand, the instrumented bridge must be flexible enough for the axle force to induce a significant strain response. On the other hand, it cannot be too long due to the impossibility of locating each axle on the bridge or distinguishing their individual contribution to the measured response accurately. Therefore, spans shorter than 20 m are generally preferred although spans up to 40 m can be used if accuracy of individual axles is not an important issue [Žnidarič and Baumgartner 1998]. Compared to conventional WIM, Bridge WIM sensors are better protected from environmental and traffic aggressiveness, they can be installed with minimum (if any) interruption of the traffic flow, and they are able to measure the load effect due to the vehicle forces for a longer time period. Moses [1979] carried out the first tests on bridges to check the possibility of using them as a traffic monitoring tool. His algorithm, like most of its successors, minimises an error function, defined as the sum of the squares of the differences between measured response and expected response according to linear static theory. The bridge response is measured using strain gauges under the bridge soffit and the theoretical static response is calculated based on the concept of influence lines, i.e., the static response is the result of adding the static contribution of each individual axle, which is equal to the multiplication of the ordinate of the influence line (that depends on the axle location at each point in time) by value of the static axle weight. The measured response has static, dynamic and noise components, but the relatively long time that it takes a vehicle to cross a bridge allows for a number of oscillations above and below the true static response that compensate for each other improving the quality of the theoretical fit. In practice, the identification of the underlying static response is a difficult task due to the influence of bridge vibrations, varying nature of axle loads, the interaction between both, and possible inaccuracies in the

positioning of the vehicle on the bridge. Maybe, one of the most serious attempts for overcoming some of the inaccuracies of Moses's algorithm (i.e., noise and dynamics) has been the application of moving identification theory [Law and Fang 2001, González et al. 2008]. The latter relies on an accurate finite element model of the bridge, dynamic programming and Tikhonov regularisation to obtain the entire time-history of each applied force. Experimental tests have shown the potential of this approach to predict accurate forces [Rowley et al. 2009], although it is acknowledged that it requires a large computational effort (calculations in real-time are typically unfeasible) and that in some cases, the calibration of the mass, stiffness and damping matrixes of the bridge model may become costly and impractical. For these reasons, Moses' algorithm remains the preferred algorithm for commercial Bridge WIM systems [Snyder 1992, Žnidarič et al. 2002], providing an acceptable solution for statistical studies of individual static weights in suitable bridges (e.g., approximately 90% of 156 axles within 15% of their true value in a 30 m continuous two-span integral bridge as part of the Cold Environmental Test [McNulty and OBrien 2003]), and a somewhat more accurate Gross Vehicle Weight (GVW) due to tendency of the errors individual axles to compensate for each other (e.g., 96.6% of 95 vehicles fell within 10% of their true value as part of the Cold Environmental Test [McNulty and OBrien 2003]). While Moses' algorithm continues to be the basis for a Bridge WIM system, hardware and software developments have contributed to the improvement in Bridge WIM results, i.e., through the use of high-resolution mechanical strain amplifiers under the bridge soffit (that can also be used as axle-detectors in suitable sites removing the need for anything on the road [Žnidarič et al. 1999a, Chatterjee et al. 2006]), optimisation [Dempsey et al. 1999] and filtering techniques that allow removal of noise and dynamics and the calculation of weights in real time [Žnidarič et al. 2002] or the use of an influence line obtained experimentally as opposed to a theoretical shape from a structural model [Žnidarič et al. 2002]. Moses initially tested Bridge WIM systems on beam-and-slab bridges and nowadays, they can also be found successfully implemented in culverts [Peters 1986], integral bridges [McNulty and OBrien 2003] and slab decks [Žnidarič et al. 1999b].

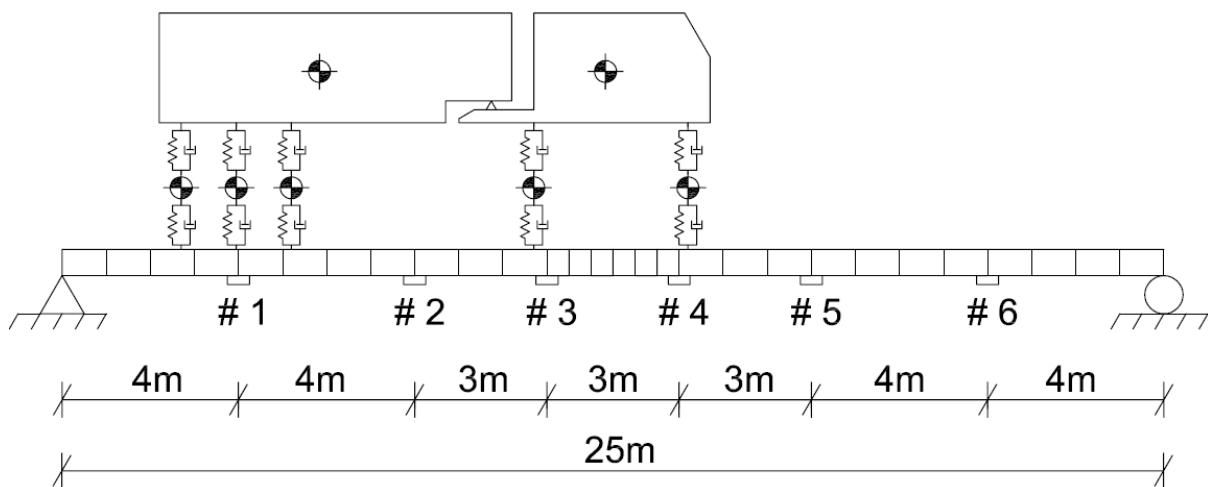
The paper here presents an algorithm that uses multiple longitudinal measurement locations to provide an instantaneous calculation of axle weights, i.e., a time-history for each axle force as opposed to a single value as in Moses' algorithm. A key feature is the exclusion of large portions of the strain record based on the value of determinant of the system of equations, used as an estimator of the state of conditioning. Compared to moving force identification solutions, the proposed algorithm is based on a set of empirical equations (there is no need for a sophisticated finite element structural model) that can be easily calibrated on site from the strain response due to a number of truck crossings. The algorithm is tested using the response of theoretical simulations based on a vehicle-bridge interaction model, and also field measurements from a 32 m long simply-supported beam-and-slab bridge located in Slovenia.

2. Development of the Algorithm

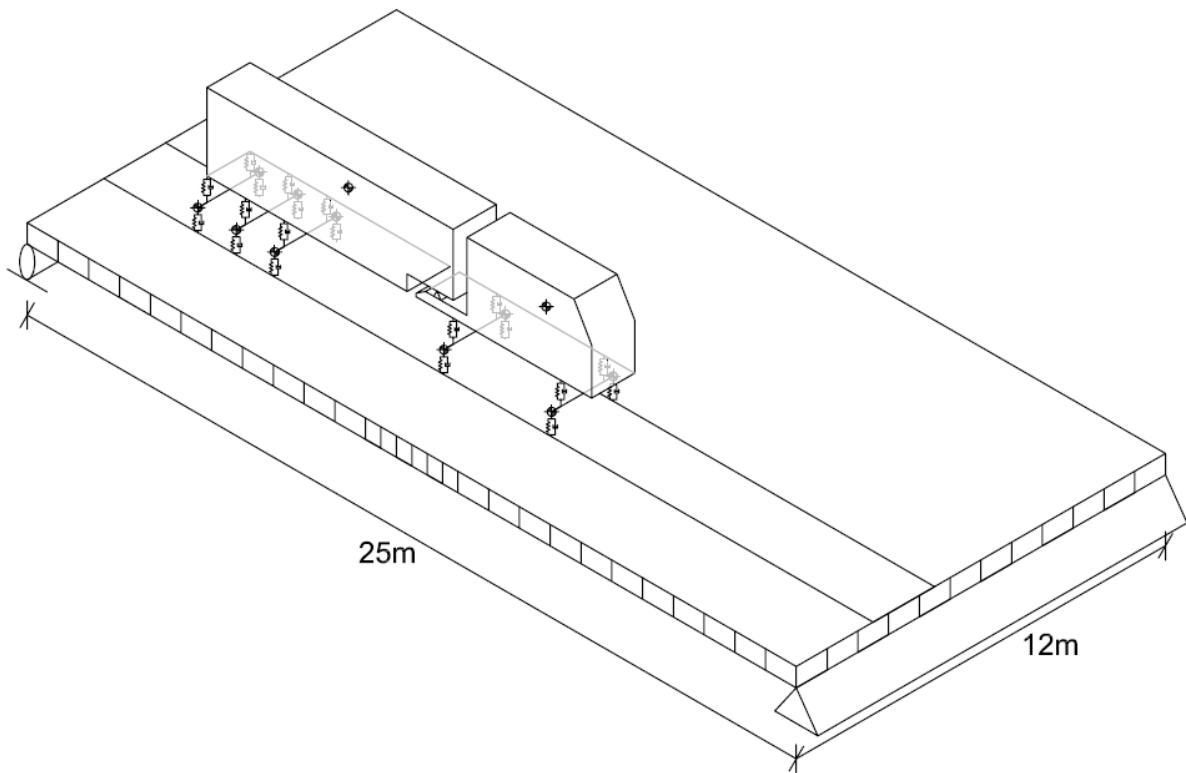
Prior to the description of the proposed Bridge WIM algorithm, the VBI model used in the simulations is presented. The theoretical strain responses of a 25 m simply supported plate model to the crossing of typical European 5-axle trucks are then employed for development and testing of the algorithm.

2.1 Vehicle-Bridge Interaction Model

The theoretical Bridge WIM testing site is assumed to have a 25 m long span and 12 m width, and it is modelled as a simply-supported plate bridge model, taking plate properties equivalent to those of a bridge section of similar span, i.e., plate thickness = 1.40 m, plate density = 1800 kg/m³, Poisson's ratio = 0.20, longitudinal modulus of elasticity = 35×10^9 N/m², transverse modulus of elasticity = 14×10^9 N/m² torsional modulus of elasticity = 9.3×10^9 N/m². The first five longitudinal modes of vibration are 4.4, 11.4, 17.8, 27.5 and 35.6 Hz, and modal damping of 3% is used, which applies the same dissipation to all modes of vibration [Yang 2005]. The bridge finite element model consists of 336 rectangular, C₁ conforming orthogonal plate elements, and it is built using Matlab [2003] [Cantero et al. 2011]. The geometry of the finite element mesh is shown in the elevation of Figure 1 (a), taking 1 m elements in the transverse direction. Strain measurements are simulated at longitudinal locations of 4 m, 8 m, 11 m, 14 m, 17 m and 21 m from the left hand support, and at 1 m, 3 m, 5 m, 7 m, 9 m and 11 m from the right-hand side in the transverse location.



(a) Elevation showing sensor locations and vehicle schematic



(b) Isometric view of the vehicle and bridge model showing vehicle path.

Figure 1. Schematics of vehicle bridge interaction model.

A 5-axle truck is modelled as two major bodies, each one representing the tractor and trailer, connected by a hinge, and 10 spring-dashpot systems representing the wheel/suspension assembly. The three dimensional model has a total of 15 degrees of freedom: one vertical hop for each wheel assembly; bounce, pitch and roll of the tractor body mass; bounce and pitch of the trailer body mass (Figure 1). This vehicle model is similar to many used previously for vehicle-bridge interaction modelling [Gillespie et al. 1979, El-Madany 1988, Wang and Huang 1992, Cebon 1993]. The Newmark- β direct integration scheme [Tedesco et al. 1999] is used to solve the vehicle system equations and calculate the vehicle response over the road profile. The vehicle and bridge equations are solved in an iterative procedure as described by Cantero et al. [2011]. The method is computationally very efficient and it has shown good agreement with other available techniques to implement the interaction between the vehicle and bridge [González 2010]. A road surface profile is incorporated into the numerical simulations in the form of a numerically generated ‘carpet’ profile. The profile is generated stochastically based on the ISO8608 [1995] method of representing road surface roughness with a power spectral density function and then applying the inverse Fast Fourier Transform [Cebon and Newland, 1983]. A Moving Average Filter (MAF) is applied to the profile, over a distance of 0.24 m [Harris et al. 2007] to simulate the tyre contact patch. The profile used is class ‘A’ (very good) and the first 40 m of the road carpet is depicted in Figure 2. The full profile generated is much longer to allow for a 100 m approach length before the vehicle enters the bridge.

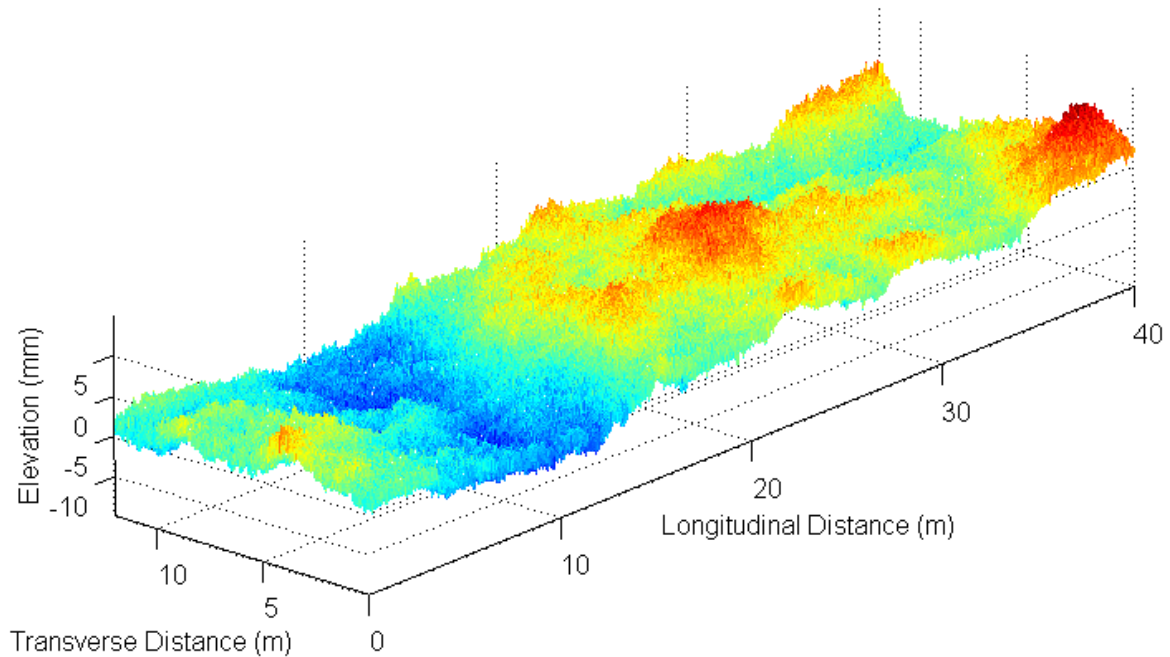


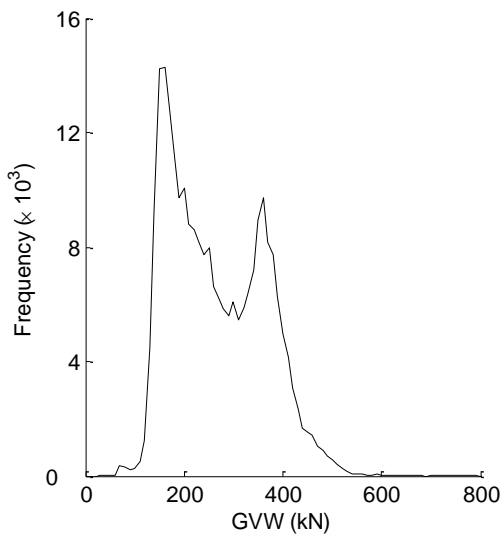
Figure 2. Section of Carpet Profile.

GVW, axle loads, axle spacings and velocities are generated, using Monte-Carlo simulation, directly from data recorded for 5-axle trucks (typical European configuration with a rear tridem) at a WIM site near Woerden, 30 km east of the port of Rotterdam in the Netherlands [ARCHES 2009]. Data was analysed for two of the three westbound lanes of the 6-lane A12 (E25/E30) highway for the 20-week period from 7th February to 25th June, 2005. Data were analysed for a total of 664,343 trucks weighing 3.5 t or more. Figure 3 shows the histograms of GVW, axle loads, axle spacings and velocity. The distance between the left and right wheels of the vehicles was 2 m. Simulating truck properties directly from the measured data removes the need to fit bi- or tri-modal distributions to the data.

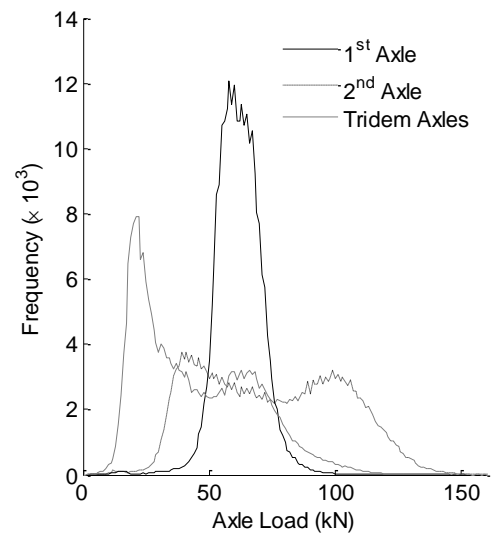
Those vehicle properties affecting the dynamics the vehicles were varied using Monte-Carlo simulation based on values found in the literature [Kirkegaard et al. 1997, Wong 1993, Fu and Cebon 2002, Harris et al. 2007]. These properties are assumed to follow a normal distribution of mean and standard deviation described in Table 1. (Note maximum and minimum values imposed so as to ensure logical vehicle configurations.)

2.2 Description of the Algorithm

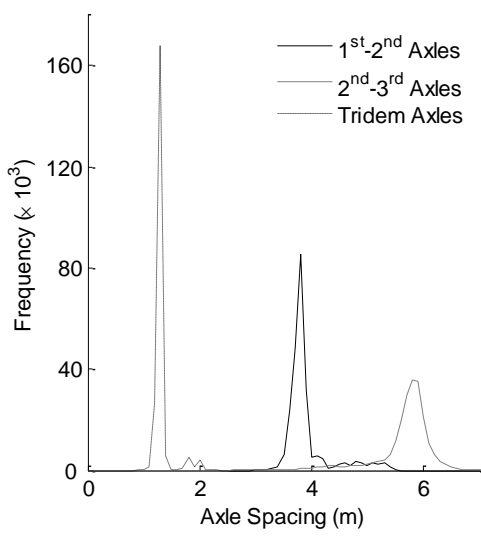
Bridge WIM systems generally use strain measurements taken at mid-span in the calculation of static axle weights. A number of sensors are placed across the mid-span section and their readings are added together to compensate for small variations in lateral position of the truck. Then, Moses' algorithm is applied to calculate that single value for each axle that minimises differences between the measured response and the theoretical static response, according to the influence line of strain at mid-span. However, this single value does not necessarily



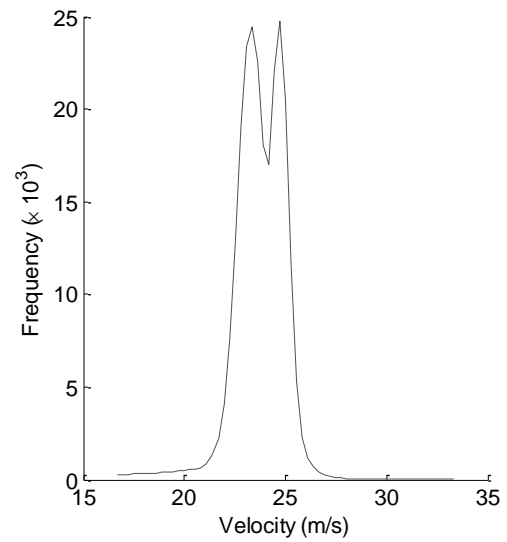
(a)



(b)



(c)



(d)

Figure 3. (a) GVW histogram; (b) Axle Load histograms; (c) Axle spacing histograms; (d) Velocity histogram recorded from the site near Woerden.

Table 1. Tyre and suspension parameters.

| | | Steer axle | | Drive axle | | Trailer axle | |
|--|-------|-------------------|-------------------|-------------------|-------------------|--------------------|-------------------|
| | | Mean | St. Dev. | Mean | St. Dev. | Mean | St. Dev. |
| Axle mass [kg] | | 700 | 100 | 1000 | 150 | 800 | 100 |
| Suspension Stiffness Coefficients [N/m] | Air | 300×10^3 | 70×10^3 | 500×10^3 | 50×10^3 | 400×10^3 | 100×10^3 |
| | Steel | 300×10^3 | 70×10^3 | 1×10^6 | 300×10^3 | 1.25×10^6 | 200×10^3 |
| Suspension Viscous damping coefficients [Ns/m] | | 5×10^3 | 2×10^3 | 5×10^3 | 2×10^3 | 5×10^3 | 2×10^3 |
| Tyre stiffness coefficients [N/m] | | 735×10^3 | 200×10^3 | 735×10^3 | 200×10^3 | 735×10^3 | 200×10^3 |
| Tyre Viscous damping coefficients [Ns/m] | | 3×10^3 | 1×10^3 | 3×10^3 | 1×10^3 | 3×10^3 | 1×10^3 |
| | | Min. | Max. | Min. | Max. | Min. | Max. |
| Axle mass [kg] | | 500 | 1000 | 7000 | 1300 | 600 | 1000 |
| Suspension Stiffness Coefficients [N/m] | Air | 150×10^3 | 500×10^3 | 300×10^3 | 600×10^3 | 250×10^3 | 600×10^3 |
| | Steel | 150×10^3 | 500×10^3 | 600×10^3 | 1.5×10^6 | 1.0×10^6 | 1.5×10^6 |
| Suspension Viscous damping coefficients [Ns/m] | | 3×10^3 | 10×10^3 | 3×10^3 | 10×10^3 | 3×10^3 | 10×10^3 |
| Tyre stiffness coefficients [N/m] | | 500×10^3 | 1.5×10^6 | 500×10^3 | 1.5×10^6 | 500×10^3 | 1.5×10^6 |
| Tyre Viscous damping coefficients [Ns/m] | | 2×10^3 | 10×10^6 | 2×10^3 | 10×10^6 | 2×10^3 | 10×10^6 |

correspond to the static component of the axle force. The minimisation procedure has difficulties in distinguishing the individual contribution of each axle to the measurement and a significant error can develop for very closely spaced axles and high speeds. Therefore, results are more accurate if the total force applied by tandems or tridems is assumed to be equally distributed between axles, i.e., axle groups are treated as only one unknown when applying the algorithm. The latter is a reasonable assumption, since it is common in trucks of this age to have load sharing mechanisms on groups of axles, such as tandems and tridems, to distribute the load equally among the axles [Cebon 1999]. High speeds may induce a small number of dynamic oscillations that the minimisation procedure is unable to compensate for, leading to poor static adjustments and large inaccuracies. In spite of these limitations, the estimation of GVW is generally accurate, while front and rear axles tend to be under-weighted and overweighted respectively. The algorithm proposed in this paper intends to improve the prediction of static weights by instrumenting multiple longitudinal sections and allowing for an instantaneous calculation at each point in time. A static equation can be established for each instrumented section and the resulting system of equations can be solved for the unknown axle forces once the number of independent equations is equal or larger than the

number of axles on the bridge. The implementation of such a system would not represent a considerable investment in relation to the more and more popular free-of-axle detection Bridge WIM systems, which are already using additional off-mid-span strain sensors, usually at $\frac{1}{4}$ -span and $\frac{3}{4}$ -span, as axle detectors [Žnidarič et al. 1999a].

2.2.1 Extension of the Original Bridge WIM Algorithm to an Instantaneous Multiple-Sensor Algorithm

Bridge WIM algorithms take advantage of the fact that vehicles are in contact with the measuring device, the bridge, for a long period of time and hence there will be many measurements available. Static algorithms based on Moses [1979] formulate, and then minimise an error function defined as in Equation (1). This error function is represented as E , where S is the total number of scans, k is scan number, ε_k^m is measured strain at scan k and ε_k^t is theoretical strain at scan k .

$$E = \sum_{k=1}^S (\varepsilon_k^m - \varepsilon_k^t)^2 \quad (1)$$

The calculation of the theoretical strain is based on linear superposition and uses the concept of static influence lines. For the case of ‘ n ’ axle static weights, represented by W_1, W_2, \dots, W_n with axle spacings of a_1, \dots, a_{n-1} , and front axle located at a distance d from the left hand support, the theoretical strain for a particular point in time would be given by Equation (2).

$$\varepsilon_k^t = W_1 I(d) + W_2 I(d-a_1) \dots + W_n I(d-a_1-\dots-a_{n-1}) \quad (2)$$

The influence line ordinate at the location $(d-a_1)$, is shown as $I(d-a_1)$ in Equation (2). Then, the axle weights are inferred by minimising the error function with respect to the unknown axle weights.

$$\frac{\partial E}{\partial W_1} = 0, \quad \dots \quad \frac{\partial E}{\partial W_n} = 0 \quad (3)$$

The result is a set of simultaneous equations where the only unknowns are the desired axle weights. Equation (4) shows the resulting system of equations.

$$\mathbf{F}_{n \times n} \mathbf{W}_{n \times 1} = \mathbf{B}_{n \times 1} \quad (4)$$

\mathbf{F} is a matrix of influence line ordinates, shown in Equation (5), where t_k is the time at scan k , and v is velocity.

$$F_{ij} = \sum_{k=1}^S I\left(t_k - \frac{\sum_{m=1}^{i-1} a_m}{v}\right) I\left(t_k - \frac{\sum_{m=1}^{j-1} a_m}{v}\right) \quad (5)$$

The vector \mathbf{B} is a product of measured strains and influence line ordinates, shown in Equation (6).

$$\mathbf{B}_i = \sum_{k=1}^S \varepsilon^m(t_k) I(t_k - \frac{\sum_{m=1}^{i-1} a_m}{v}) \quad (6)$$

However, it has been reported in the literature [OBrien et al. 2009, Deesomsuk and Pinkaew 2009] that the Bridge WIM equations are commonly ill-conditioned, i.e., small changes in the coefficients of the solution have severe effects on the results. The determinant is often used as an indicator of the condition of a system of equations, and in the case of the Bridge WIM equations the determinant of \mathbf{F} approaches zero as the degree of ill-conditioning increases. There are many methods of improving the condition of a system of equations [Kim et al. 1996, Xue et al. 2000], and these methods generally involve manipulating the system of equations in such a way that it is the solution of a nearby, and better conditioned, system that is actually solved for. The most widespread example of this type of method would be Tikhonov regularisation [Tikhonov and Arsenin 1977], and a system of regularised Bridge WIM equations has been proposed by OBrien et al. [2009] that slightly improves results. The latter consists of minimising a new objective function given by Equation (1) plus an additional penalty term multiplied by a regularisation parameter λ . If λ is equal to zero, the problem is that of the classic Moses' algorithm. The purpose of adding the term in λ is to reduce the ill-conditioning of the system and consequently reduce the error inherent in Moses' equations.

The algorithm proposed herein does not solve a single system of equations as in Equation (4), but a simultaneous set of equations for each scan, based on the readings of sensors at multiple longitudinal locations. At each scan k , the system of equations shown in Equation (7) are defined, i.e., \mathbf{G} , \mathbf{X} and \mathbf{C} are time-varying matrices. For each scan, a set of axle forces can be obtained from the system of equations once the number of instrumented sections equals or exceeds the axles on the bridge. In this way the algorithm produces a force history for each axle.

$$\mathbf{G}_{n \times n}^k \mathbf{X}_{n \times 1}^k = \mathbf{C}_{n \times 1}^k \quad (7)$$

The differences between Equations (4) and (7) are that the terms are no longer summed for each scan and there are multiple sensor locations contributing in Equation (7), where there was only one location in Equation (4). The coefficient \mathbf{G}_{ij} of matrix \mathbf{G} are defined in Equation (8) where H is the total number of sensor locations and $I_h(t_k)$ is the influence line ordinate at time t_k , associated with sensor location h .

$$\mathbf{G}_{ij} = \sum_{h=1}^H I_h(t_k - \frac{\sum_{m=1}^{i-1} a_m}{v}) I_h(t_k - \frac{\sum_{m=1}^{j-1} a_m}{v}) \quad (8)$$

The vector \mathbf{C} is a product of measured strains and influence line ordinates, at each of the H sensor locations. The coefficients of \mathbf{C} are given by Equation (9).

$$\mathbf{C}_i = \sum_{h=1}^H \varepsilon^m_h(t_k) I_h(t_k - \frac{\sum_{m=1}^{i-1} a_m}{v}) \quad (9)$$

The advantage to using the readings of each scan independently, is that those points in time when the system of equations is poorly conditioned, can be removed from the final solution. Using the determinant of \mathbf{G} ($\det(\mathbf{G})$) was found to be the most robust method of indicating those scans for which the system was sufficiently well conditioned to have confidence in the predictions.

The algorithm predicts a force history based on static equations, and best results are produced when the large dynamic oscillations due to bridge inertial forces that are part of the measured total response are filtered out prior to the application of the algorithm. The system then uses only those scans for which $\det(\mathbf{G})$ is sufficiently high to estimate a history of quasi-static axle forces with high confidence levels. If dynamics due to main mode of vibration of the bridge were removed accurately, time history predictions with sufficiently high determinants should appear approximately as a horizontal straight line, except for small disturbances due to higher modes or vehicle dynamics.

2.2.2 Implementation of the proposed algorithm using a single vehicle

Figure 4 illustrates the strain simulated at six locations in response to the passage of a 5-axle truck using the VBI model described in Section 2.1. The major characteristics of the vehicle in this simulation are: 1st axle static load of 45.0 kN (all static axle loads equally distributed on each wheel), 2nd axle static load of 54.0 kN, each axle of the tridem static load of 14.0 kN;

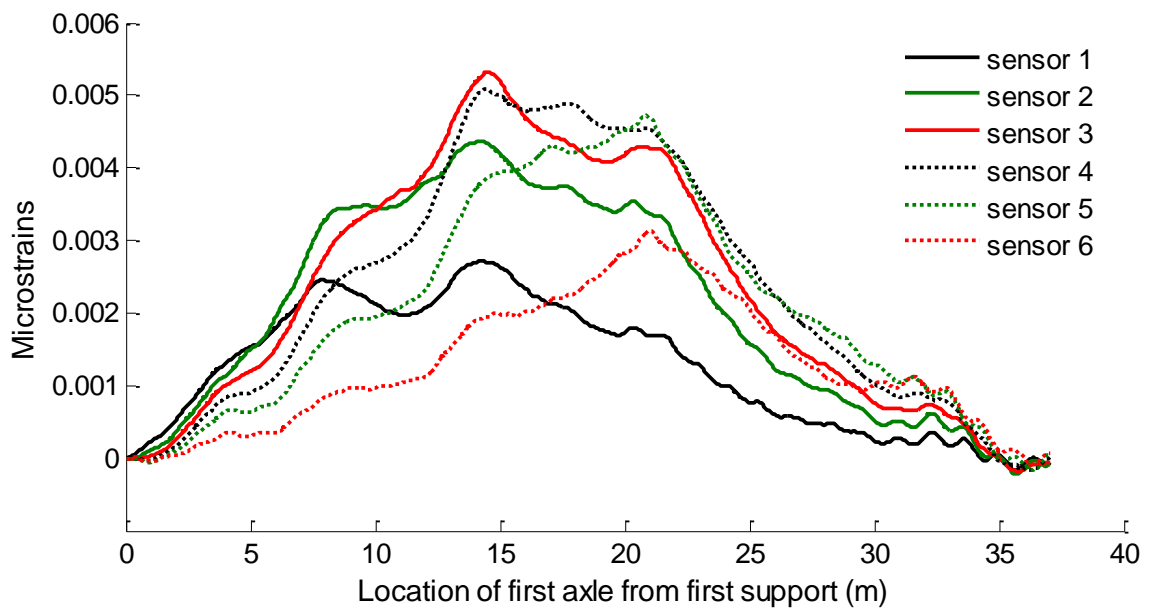


Figure 4. Simulated strain at six longitudinal sensor locations.

axle spacings of 3.8 m, 5.9 m, 1.2 m and 1.2 m between the 1st-2nd, 2nd-3rd, 3rd-4th and 4th-5th axles respectively; and velocity of 86.4 km/hr. It is decided that for vehicles with axle groups, such as those modelled here, the individual axles of these groups would carry equal static load. This reduces the number of unknowns from five to three in the case of a 5-axle vehicle (1st axle, 2nd axle and an axle of the rear tridem) and it improves the conditioning of the system and the accuracy of the results without increasing the number of instrumented sections.

The influence of bridge dynamics is minimised here by filtering the total strain response at the six longitudinal sections using a MAF before being input to the algorithm. The number of data points to be used with the MAF is based on the 1st natural frequency of the bridge. In practice, this frequency can be found from a record in free vibration of the bridge response. Here, the 1st natural frequency is 4.4 Hz, and the scanning frequency is 500 Hz. Hence the number of data points which should be used in the MAF is $(500/4.4) = 114$. The authors found the simple MAF to be the most robust filtering technique (compared to band-pass and low-pass filters) to be applied. In the application of the MAF, it is the central point of the filter span being manipulated and when filtering those points within the start and end portions of the signal, additional fictitious points before or after the signal are added to pad to the filter length. The result of applying this filtering to the simulated response is shown in Figure 5.

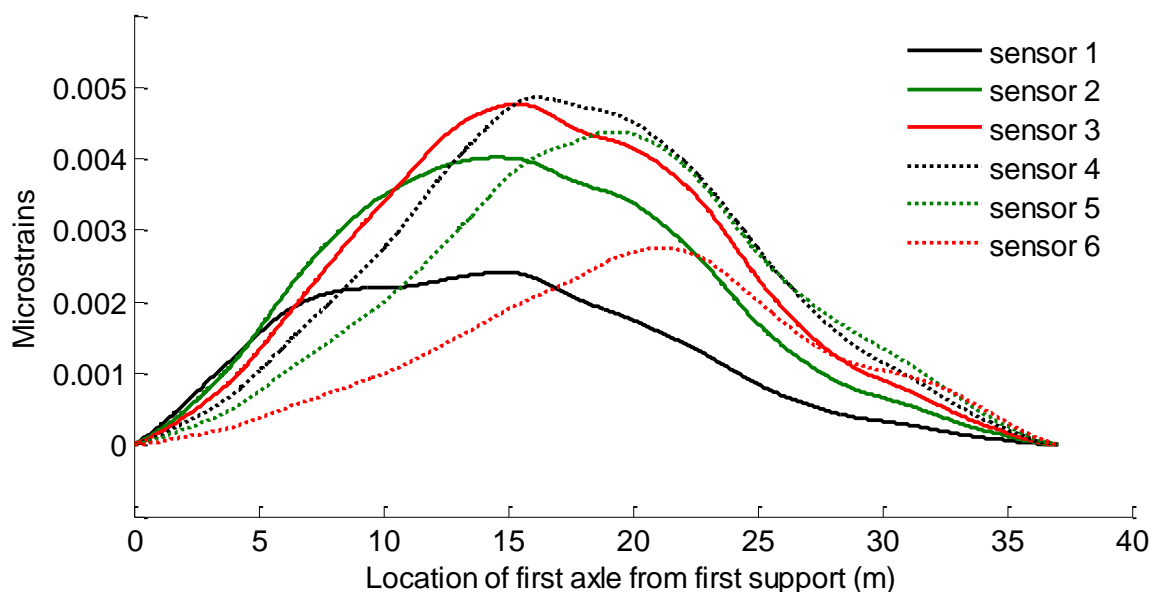
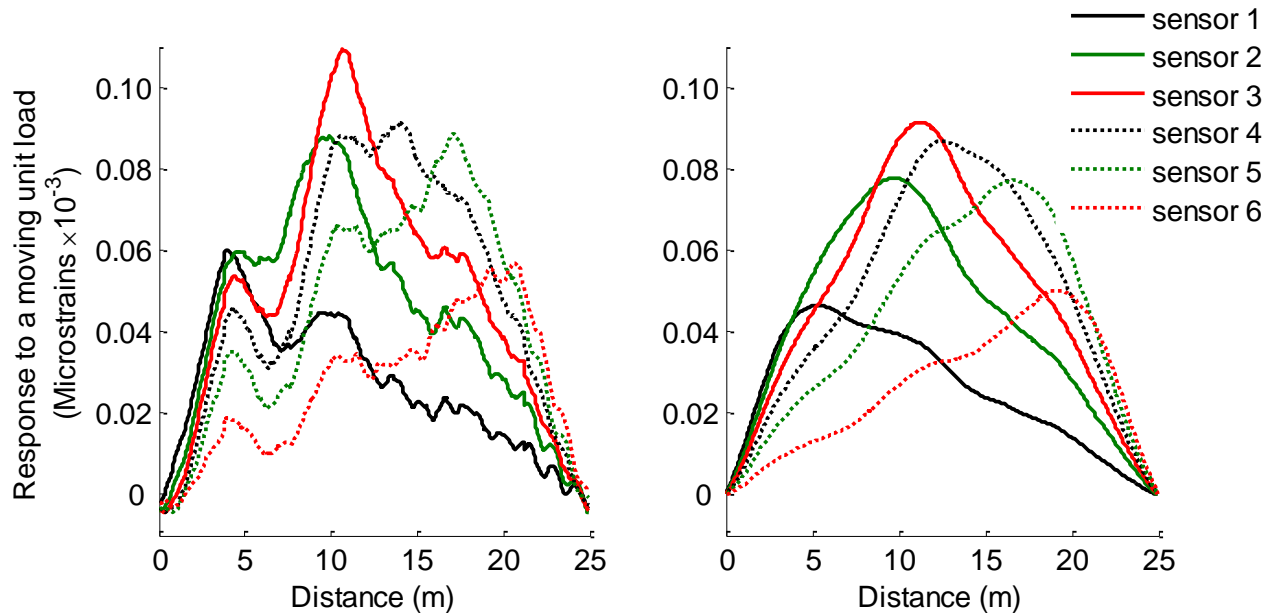


Figure 5. Strain at six longitudinal sensor locations after applying the MAF.

OBrien et al. [2006] describe a method of determining the influence line of a bridge from direct measurement, using the Bridge WIM equations and taking the influence line ordinates as the unknowns as opposed to the static axle loads that will be known for the calibration vehicle. The influence lines in Figure 6(a) were obtained using the strain measurements of Figure 4 as an example. This method is able to provide an accurate influence line directly from measurements in rigid structures, such as integral bridges or culverts, but in a general case like the bridge used here, the resulting influence line for each measurement location

would be corrupted by large dynamic oscillations. The influence of bridge dynamics is reduced here by filtering the calculated influence lines using a MAF as shown in Figure 6(b).



(a) Influence lines calculated using the optimisation procedure of OBrien et al. [2006].

(b) Influence lines after applying the MAF.

Figure 6. Calculated influence lines for the six sensor locations.

The influence lines of Figure 6(b) do not exactly follow a triangular shape as theory could suggest, but retain some oscillations of the measured strain response used to calculate them. The source of these oscillations is related to truck frequency components; remnants of the bridge 1st frequency, etc. A method to remove these deviations from the final influence lines used in the algorithm will be outlined in Section 2.2.3. For this example, the inputs to the algorithm are the filtered strains depicted in Figure 5, vehicle velocity and axle spacing and the influence lines determined during the calibration procedure (or Figure 6(b)). Figure 7 shows the force history predictions of the proposed algorithm.

There are three different lines plotted in Figure 7 for each axle: the average of the actual applied forces of the left and right wheels (dotted), the actual static wheel force (dashed) and the predicted wheel force (solid). Each of the lines is for a wheel load, or half the calculated axle load. The secondary (right hand side) y-axis refers to the value of $\det(\mathbf{G})$ (plotted with the dash-dot line-type) (Equation (8)). The vertical lines as the force predictions tend to zero and infinity correspond to an axle entering/exiting the bridge; at these locations \mathbf{G} approaches singularity and the static axle weight predictions become erratic. In the case of the classic

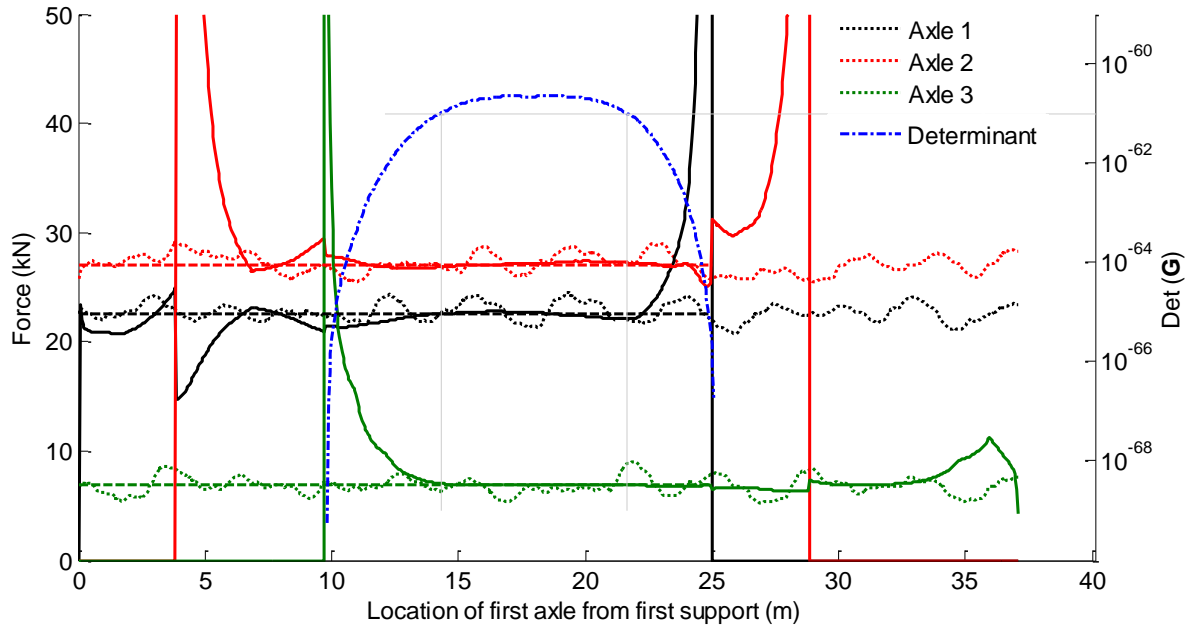


Figure 7. Force history predictions.

Moses' algorithm, these erroneous scans would contribute, with equal merit, to the total of \mathbf{F} and \mathbf{B} (Equation (4)). As \mathbf{G} approaches singularity at the erratic portions, removing such erroneous static axle weight predictions improves the overall accuracy of the algorithm. Here the minimum value of $\det(\mathbf{G})$ used to infer the static axle weight from the force prediction is chosen to be 10^{-61} (represented by an horizontal solid thin line in Figure 7), which gives bounds on the predicted force of between approximately 14.5 m and 21.5 m from the start of the bridge, represented by two vertical solid thin lines in the figure). In practice, these limits can be established using a calibration truck. Considering only that portion of the force history where the determinant has been deemed to have a sufficiently high value, the static weights are inferred averaging the predicted forces for each axle. The errors in the predicted static values of axle 1, axle 2, axle 3 and GVW are found to be -0.05%, 0.7%, 0.2% and 0.3% respectively.

The errors for this case using the classic Moses' algorithm are -1.8%, 3.4%, -1.9% and 0.2% for the static values of axle 1, axle 2, axle 3 and GVW respectively. When using the solution to the regularised Moses' equations with an optimum regularisation parameter λ [OBrien et al. 2009], errors of -1.5%, 0.2%, 2.2% and 0.3% are obtained for axle 1, axle 2, axle 3 and GVW respectively. In the latter, the optimum regularisation parameter λ has been selected using the L-Curve [Hansen 1992] shown in Figure 8(a) where the optimal λ is given by the point of maximum positive curvature (6×10^{-42}) represented in Figure 8(b). This attempt to reduce the ill-conditioned nature of Bridge WIM equations through the addition of a regularisation term is indeed an improvement on the classic Moses' algorithm, but worse in comparison with the proposed multi-sensor algorithm.

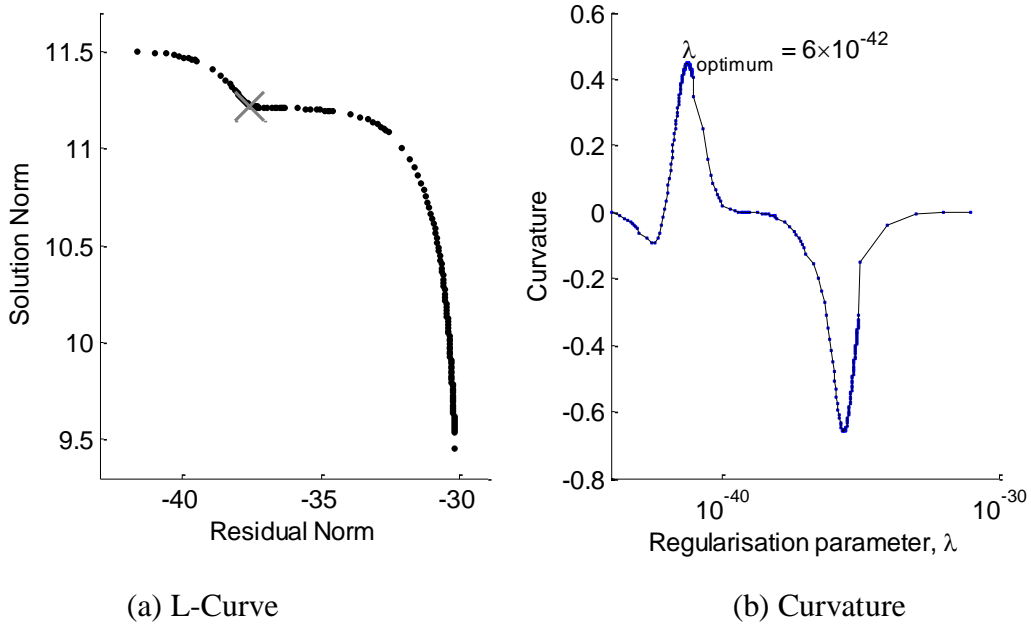


Figure 8. L-Curve and Curvature.

The matrix reciprocal condition number (Rcond) is used [Matlab 2003] to facilitate a direct comparison of the condition of the solutions using the regularised Moses' equations and the proposed algorithm. The determinant was found to be the most robust indicator with regard to solution stability, but the determinant of one system of equations cannot be directly compared to that of another. The magnitude of the determinant of a matrix can vary significantly from one system to another, i.e. two systems that are equally conditioned may have drastically different values of determinant due to the relative scales of the coefficients involved in constructing the matrices in each case. Values of Rcond will always lie between 0, indicating singularity, and 1, making it a natural choice for comparative purposes.

Figure 9 shows the effects of the regularisation on the condition of the Bridge WIM equations. For varying λ values, the resulting errors in the predicted static weights are shown on the primary y-axis, and the Rcond value of the system is shown in the secondary y-axis. The classic Moses' algorithm is equivalent to regularised Moses with a λ value of zero and adding progressively larger λ values, solves for a neighbouring, and sometimes better conditioned solutions. In this case, λ values $< 1 \times 10^{-44}$ have no effect on the solution and are essentially equal to the predictions of classic Moses. The Rcond value of classic Moses is 1.6×10^{-7} . The regularised solutions improve to peak-accuracy predictions at the optimum λ value of 6×10^{-42} , with an Rcond (Rcond of \mathbf{F}_{reg}) value of 1.6×10^{-6} , but from here improvements in the condition of the system are at a detrimental cost to the accuracy of the results. In comparison, the Rcond values of those \mathbf{G} matrices used in calculating static weights of the proposed algorithm (those scans for which $\det(\mathbf{G}) > 1 \times 10^{-61}$) have a minimum Rcond of 3.6×10^{-4} .

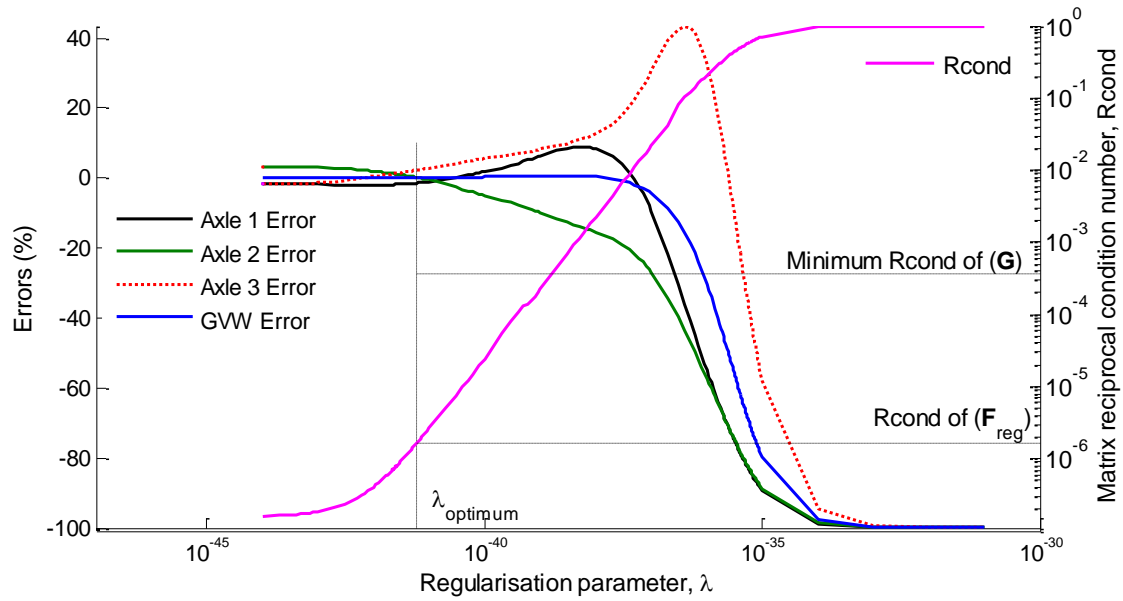


Figure 9. Force history predictions.

2.2.3 Calibration of the Algorithm

The calibration procedure consists of defining the influence lines that will be used in the algorithm and setting the limit for the determinant to be used in calculations. The determination of an appropriate influence line is crucial to the success of the algorithm. Recommendations in the COST323 specification [COST323 2002] for ‘extended repeatability conditions’ consist of driving a single calibration vehicle over the bridge at a range of speeds and for three loading conditions: empty, half-loaded and fully-laden. Throughout this study comparisons to Moses’ classic algorithm refer to a system calibrated in this way. A different but similarly simple procedure is adopted here. This procedure uses randomly selected trucks from ambient traffic (velocity, axle weights and spacings and dynamic properties sampled from the theoretical distributions in Section 2.1) as opposed to a designated calibration vehicle. The optimisation algorithm of OBrien et al. [2006] is applied to the measured strain responses of the vehicles from ambient traffic and the influence lines are determined for all the longitudinal locations. For each longitudinal location, the average of all the influence lines obtained for the simulated vehicles is calculated and the MAF filter is applied to give the final set of influence lines to be used in the algorithm.

Figure 10 shows how the influence lines calculated for sensor locations 2 and 6 (Figure 1(a)) vary using different numbers of trucks from traffic. Other sensor locations are omitted in the figure for clarity. There are five lines in both Figures 10(a) and (b), the influence line calculated using the optimisation algorithm of OBrien et al. [2006] for a single truck, the average of the influence lines calculated for two trucks and the averages calculated for five, ten and twenty trucks. The vehicle parameters were selected using Monte-Carlo simulation from the distributions described in Section 2.1. The velocities of the trucks, for example, ranged from a minimum of 75 km/hr to a maximum of 90 km/hr.

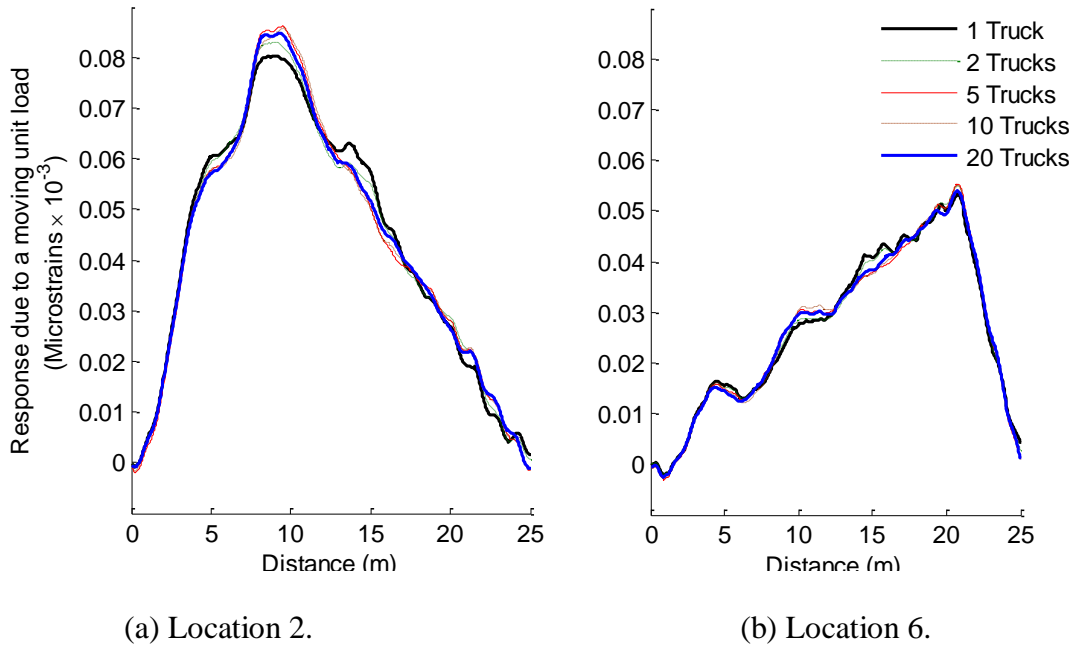


Figure 10. Average influence lines calculated using different numbers of trucks.

The influence lines calculated in Figures 10(a) and (b) converge to a representative response quickly. The dominance of the bridge 1st frequency dynamic component can be seen in the initial portions of the influence line. With the averages of the influence lines obtained, the last step is to apply the MAF. The MAF is designed to encompass the number of data points corresponding to the period of the bridge 1st frequency, as mentioned in Section 2.2.2. The results of applying the MAF are shown in Figure 11.

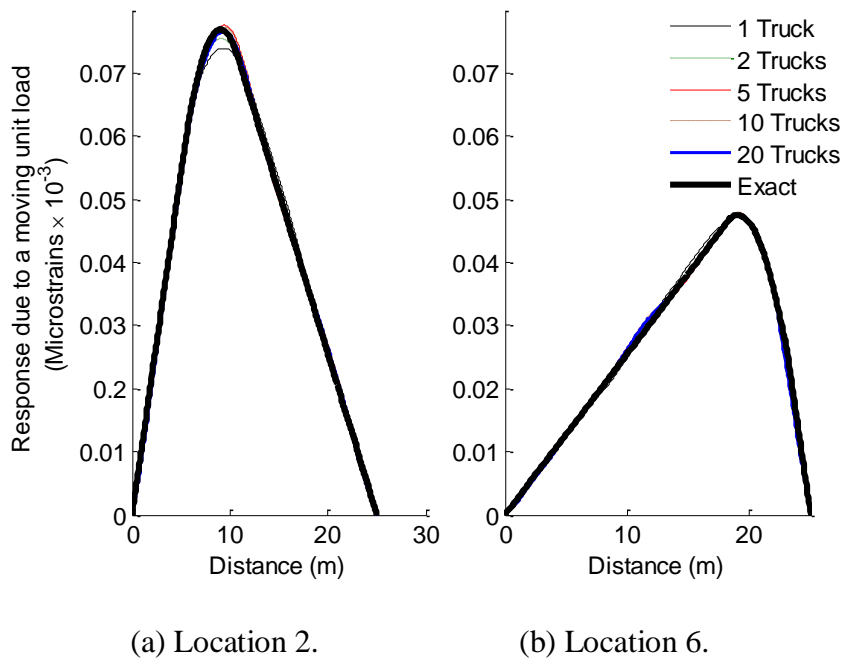


Figure 11. Average influence lines calculated using different numbers of trucks after applying a MAF.

A major advantage of the theoretical simulations here is that the exact answer to the problem at hand is readily available. The exact filtered static influence lines are plotted in Figure 11 to compare to the filtered average calculated influence lines. It can be seen that there is a very good match between the exact influence lines and those calculated using 10 or 20 trucks. This calibration procedure could be the case of a weighing campaign carried out by the police where the static weights of random trucks that have crossed or are about crossing the bridge are measured using portable weighing scales or similar.

The MAF filter is applied as the last step in the algorithm deliberately. The alternative to applying the MAF at this stage is filtering the measured strains before calculating the influence line, which is less effective. The reason for this is that the optimisation algorithm of O'Brien et al. [2006] can produce influence lines with local discontinuities due to the numerical optimisation procedure (these are not easy to distinguish in Figure 10 due to high levels of dynamics present), and hence if the MAF was applied to the measured strain before calculating the influence lines, a second MAF would have to be applied to the influence lines to remove these local discontinuities. The method loses robustness with increasing demand for manipulation of the signal. Secondly, as can be seen in Figure 10, averaging the influence lines calculated using the unfiltered strain signals of different trucks, removes much of the high frequency dynamic components. These higher frequency components can, in places, reduce the effectiveness of the MAF, and hence having much of the higher frequency dynamics reduced or removed before the application of the MAF is beneficial to the final output of the algorithm.

Figure 12 shows how a change in the number of trucks employed in the calibration affects the overall accuracy of the multiple-sensor Bridge WIM algorithm using a sample of 100 trucks as a test population. The test population is distinct from the population used to generate the influence lines and is generated using Monte-Carlo simulation from the distributions described in Section 2.1. The primary y-axis measures the sum of the squared differences between the influence line obtained using n trucks and the influence line obtained using $n-1$ trucks. There are six solid lines, one for each of the six section longitudinal locations. For the characteristics of this truck population, the average of the influence lines converges after about 20 trucks used for calibration (as is seen in Figure 10), but the results of a calibration procedure using up to 40 trucks is included for thoroughness. Using further runs to calculate the influence line has virtually no effect after this point. The secondary y-axis shows the standard deviation of the error in individual static axle weights obtained with the influence line calibrated with n trucks and it is represented with symbols in the figure. The mean values of the errors plotted are 0.6%, -2.2%, 1.1% and -0.4% for the 1st axle, 2nd axle, 3rd axle and GVW categories respectively for the case of 40 trucks used in the calibration.

The minimum value of $\det(\mathbf{G})$ that qualifies for weight calculations is the final parameter to be established during calibration. In choosing this value, a compromise must be sought between setting the limit sufficiently high so as to have a well-conditioned set of system equations, and hence a high degree of confidence in the solution, and setting the limit sufficiently low so as to have a force history prediction long enough to work with. Bridge

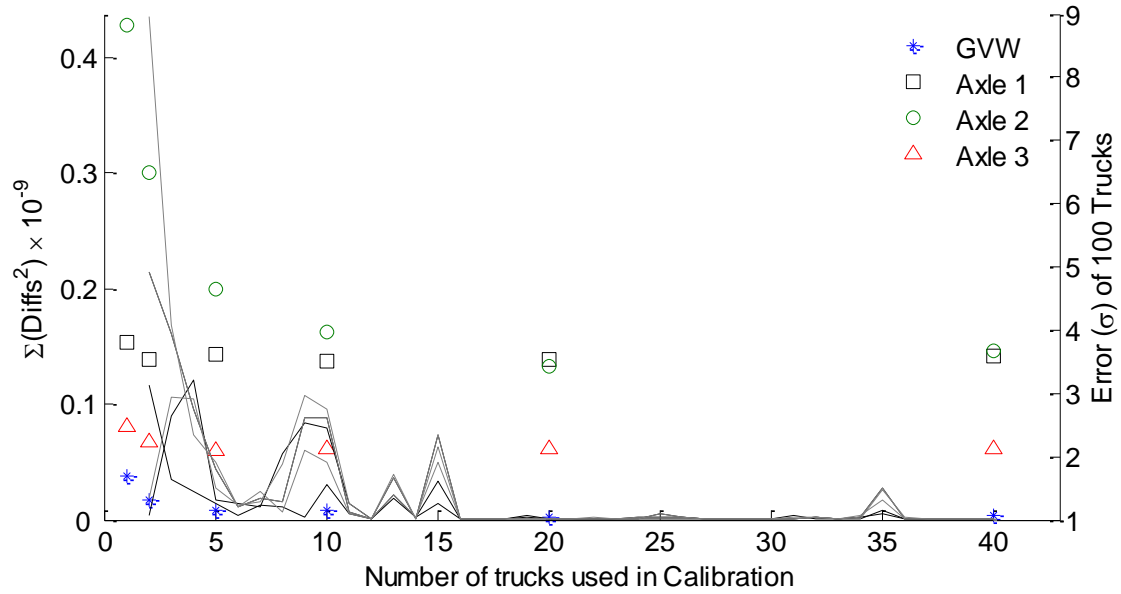


Figure 12. Number of trucks used in calibration Vs Errors in predicted axle weights.

WIM systems are known to be more accurate in their prediction of GVW than individual axles. The more critical category of errors in individual static axle weights is presented in Figure 13 for a sample of twenty trucks versus the limit of $\det(\mathbf{G})$ corresponding to six longitudinal sensor locations.

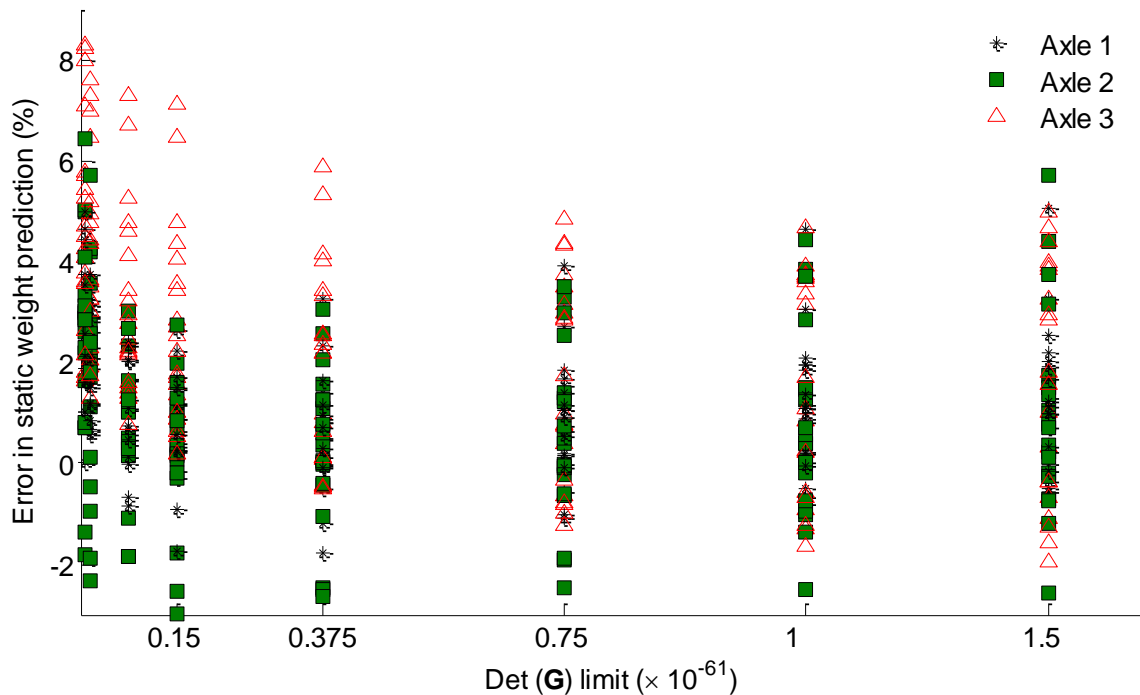


Figure 13. Optimum limit of $\det(\mathbf{G})$.

From this analysis, the optimum limit of $\det(\mathbf{G})$ is 1×10^{-61} , that corresponds to approximately 6.5 m of the force history predictions used in the final calculations of the static weights. Other $\det(\mathbf{G})$ values of 0.15×10^{-61} , 0.375×10^{-61} , 0.75×10^{-61} and 1.5×10^{-61} shown in the figure

correspond to lengths of force history predictions of approximately 10.5 m, 9.5 m, 8 m and 5.5 m respectively, and they lead to a poorer estimation of weights.

2.3 Influence of number of longitudinal locations

The simulations presented so far have focussed on six longitudinal locations along the bridge (Figure 1(a)). Figure 14 compares the force history predictions and $\det(\mathbf{G})$ based on three (lighter line-weight) and six longitudinal sensor locations (heavier line-weight) for a randomly selected truck from traffic (using the distributions in Section 2.1). The six sensor and three sensor systems were both calibrated using 20 trucks. The major difference between the two cases is the shape of $\det(\mathbf{G})$ obtained in each case. Using the limits shown for the six sensor and three sensor algorithms (10^{-61} and 10^{-62} respectively), minimum and maximum Rcond values for the \mathbf{G} matrices considered in the solution were 0.4×10^{-3} and 2.5×10^{-3} for the six sensor case and 0.28×10^{-3} and 2.1×10^{-3} for the three sensor case. This shows that in the case of the six sensor algorithm the system equations are indeed better conditioned and for a longer period as can be seen in Figure 14. The determinant is above the specified limit for approximately 7 m for the six sensor algorithm and approximately 5.5 m for the three sensor algorithm. The format of Figure 14 is similar to Figure 7, that is, there are four lines plotted pertaining to each axle; the average of the actual applied forces of the left and right wheels (dotted), the actual static wheel force (dashed) and two predicted wheel forces (solid). As in Figure 7, each of the lines is for a wheel load, or half the calculated axle load. The light and heavy line-weight of the wheel force predictions correspond to the three sensor and six sensor algorithms respectively. The secondary (right hand side) y-axis refers to the value of $\det(\mathbf{G})$ (plotted with the dash-dot line-type, again heavier line-weight for the six sensor algorithm).

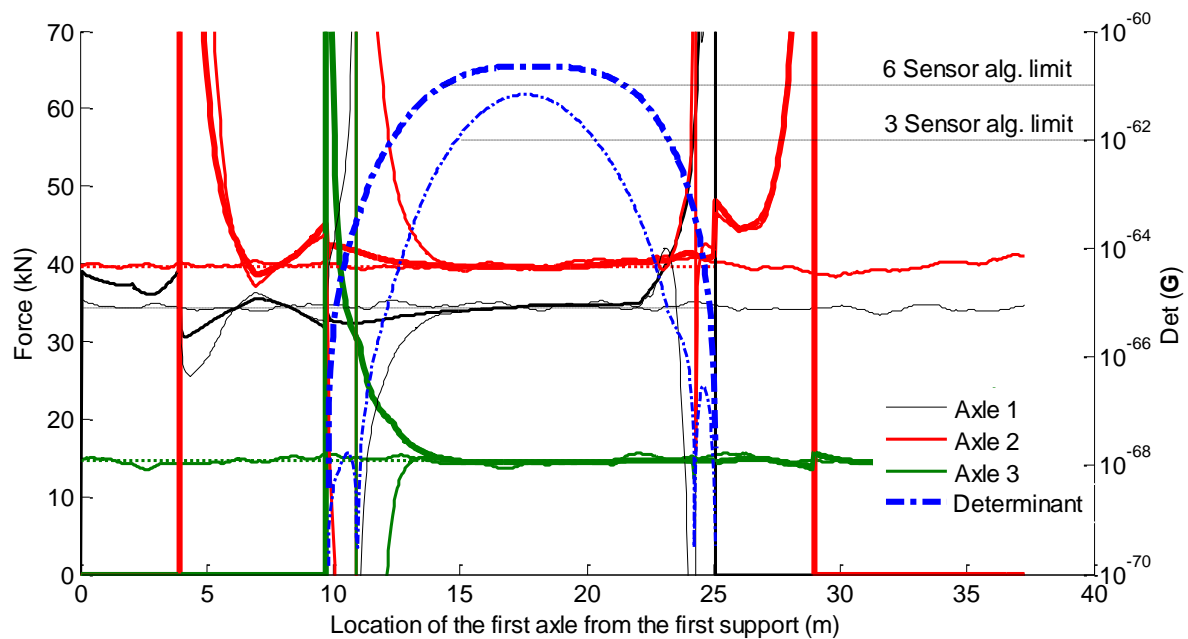


Figure 14. Force history predictions for three (dashed) and six (solid) longitudinal locations.

The errors in the predicted static weights for the truck considered in Figure 14 are 0.4%, -0.2%, -1.5% and -0.5% for axle 1, axle 2, axle 3 and GVW respectively using the six sensor algorithm. The errors for the three sensor algorithm are comparable: 0.1%, 0.1%, -2.0% and -0.7% for axle 1, axle 2, axle 3 and GVW respectively, while the classic Moses' algorithm leads to errors of -2.0%, 2.1%, 0.5% and 0.3% for axle 1, axle 2, axle 3 and GVW respectively.

The results presented in Figure 14 are for one randomly selected truck from traffic. This truck is part of a larger sample of 100 randomly selected trucks, simulated again using the distributions described in Section 2.1, used to comprehensively test the algorithm. The results of the 100 test trucks are presented in Table 2.

Table 2. Mean and standard deviation of errors for the test population using the three algorithms.

| | Axle 1 | | Axle 2 | | Axle 3 | | GVW | |
|-------------------------|--------|---------|--------|---------|--------|---------|-------|---------|
| | Mean | St.Dev. | Mean | St.Dev. | Mean | St.Dev. | Mean | St.Dev. |
| Six sensor algorithm | 0.08 | 1.77 | -0.13 | 3.20 | -0.01 | 2.09 | 0.08 | 1.29 |
| Three sensor algorithm | -0.09 | 2.05 | -0.01 | 3.23 | -0.26 | 2.78 | -0.03 | 1.62 |
| Classic Moses algorithm | -3.75 | 5.93 | 2.67 | 8.26 | 0.95 | 2.40 | 0.44 | 0.52 |

2.4 Influence of errors in vehicle velocity/axle spacing on predicted results

Errors in Bridge WIM systems can be derived from an inaccurate location of the vehicle on the bridge at each point of time as a result of poor estimations of velocity and/or axle spacing. This section analyses the sensitivity of the new algorithm to these types of errors. To show the consequences of misread axle spacing, an error of 10% (55 cm) was introduced in the spacing between the 2nd and 3rd axles. Figure 15 shows the force history predictions as solid lines for a truck randomly selected from traffic with the erroneous axle spacing measurement. The predictions in the case of the 1st and 2nd axles have deviated from the quasi-horizontal static predictions that would be expected in ideal conditions. The errors in the predicted static weights of axle 1, axle 2, axle 3 and GVW were -4.7%, 6.6%, 0.3% and 2.1% respectively. In comparison Moses errors for this case were -14.3%, 13.0%, -8.6% and 0.6% for the predicted static weights of axle 1, axle 2, axle 3 and GVW respectively.

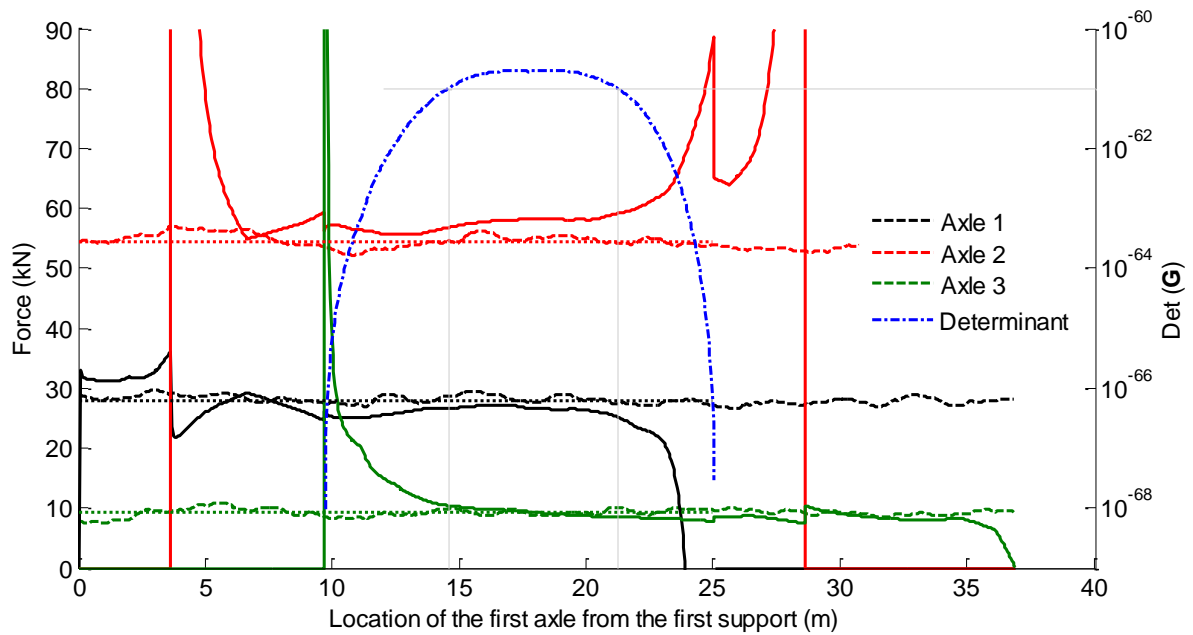


Figure 15. Force history predictions: 10% error in axle spacing.

To a similar end as the simulation of Figure 15, another simulation was run, this time with a 5% error in velocity. The force history predictions for this case are shown in Figure 16. All axles will have an inaccurate location on the bridge at each point in time, and as a result, the errors in the predicted static weights of axle 1, axle 2, axle 3 and GVW were -48.1%, 16.1%, 17.4% and 0.2% respectively. By comparison Moses errors for this case were -5.7%, -10.3%, 45.7% and 5.0% for the predicted static weights of axle 1, axle 2, axle 3 and GVW respectively.

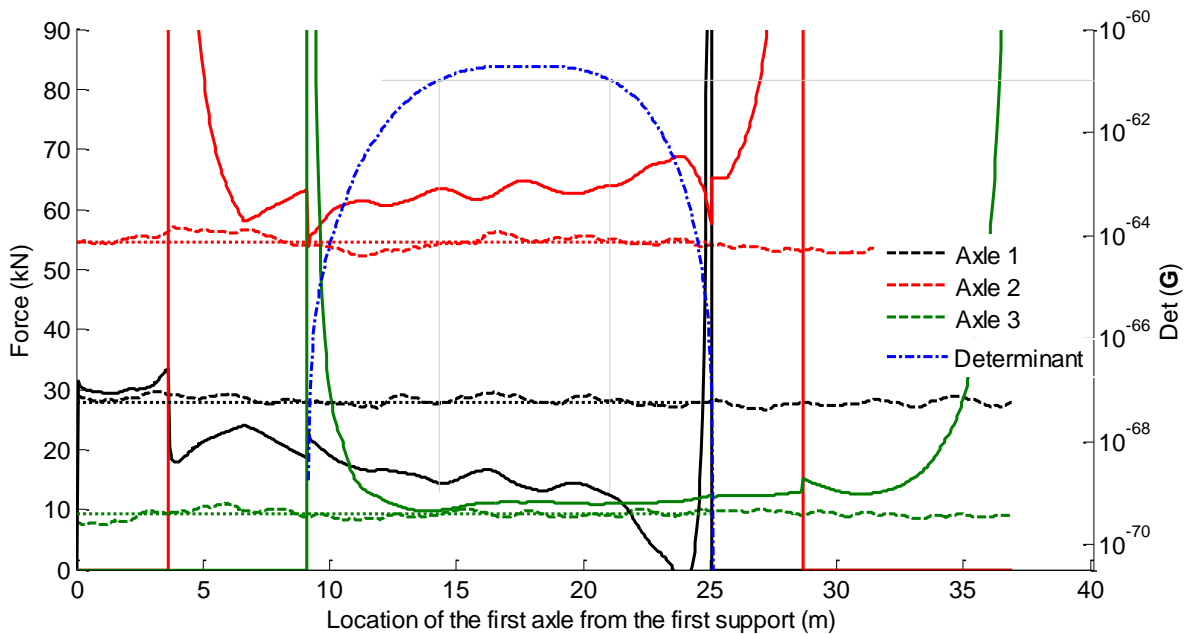


Figure 16. Force history predictions: 5% error in velocity.

It would be clearly advantageous to have, in any Bridge WIM system, a method of identifying those predictions which are likely to be erroneous, i.e., due to a poor estimation of axle spacing and/or velocity. Unlike the traditional static Bridge WIM algorithm, the multiple sensor Bridge WIM algorithm has an interesting feature that can be used for the purpose of identifying these outliers. In applying a MAF to the measured response, the algorithm is seeking to remove the effects of the dominant bridge frequencies leaving unaltered most of the underlying static component (i.e., the lowest frequency components of the signal). Hence, in ideal conditions, the force history predictions within the region of the bridge where the value of the determinant has been established to be sufficiently high should be approximately horizontal straight lines. Any significant deviation from horizontal or straight would suggest an unreliable prediction. Therefore, a straight line can be fitted to the force history prediction using least squares, and the correlation of fit and slope of this best-fit used as indicators of the robustness of the prediction. Those trucks with large slope or weak correlation of fit can then be marked as potentially erroneous. The sum of the differences squared ($\Sigma \text{diffs}^2, r$) is used as the measure of the correlation between the line of best fit and the predicted force history. Figure 17 is plotted to show how slope and correlation of fit vary with errors in velocity of 0-5%.

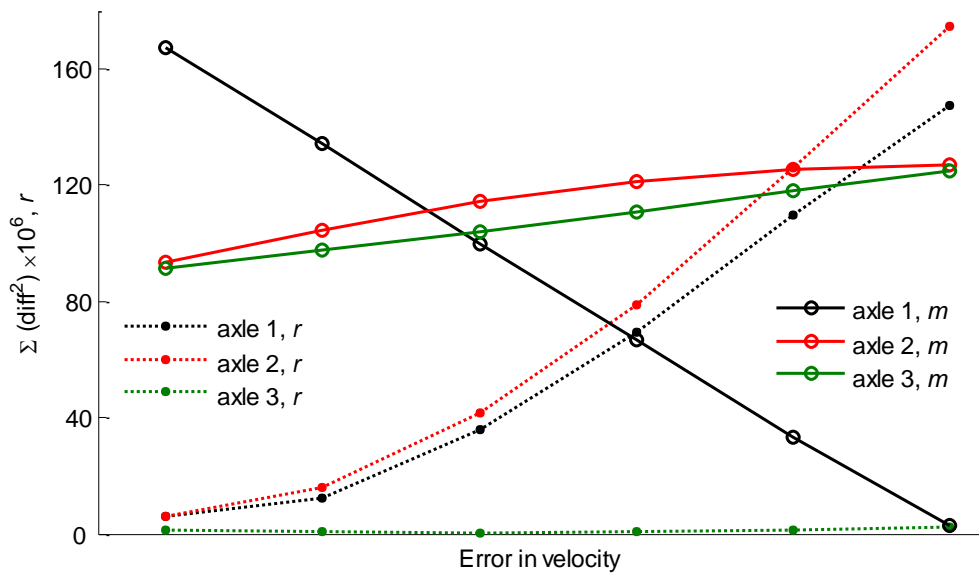


Figure 17. Force history predictions: 5% error in velocity.

For axles 1 and 2, the Σdiffs^2 increases strongly with increasing error in velocity, while this trend is not as visible for axle 3. Likewise for the slope of the line of best fit, there is a strong trend for axles 1 and 2, no noticeable trend for axle 3. Figure 17 shows that there is potential in this method of identifying potential outliers.

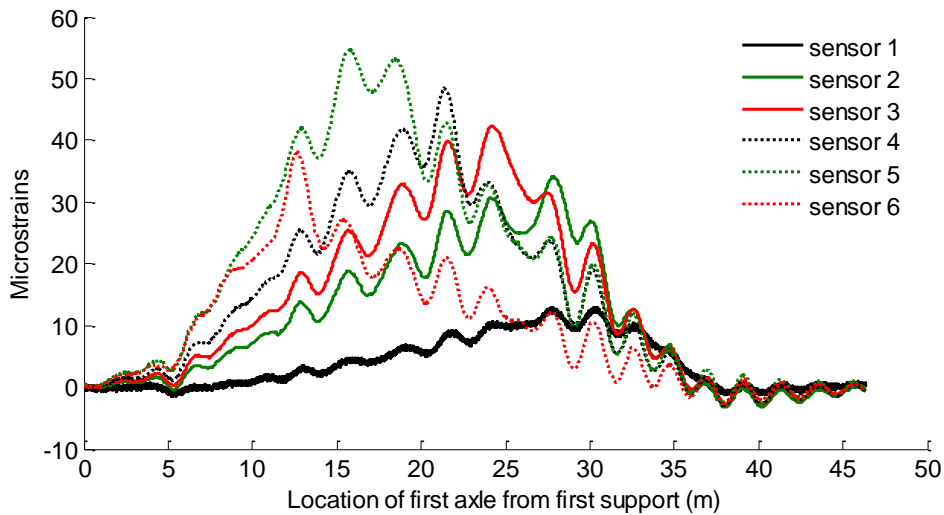


Figure 19. Measurements of the 2-axle truck travelling at 28.4 km/hr.

Once the vehicles have completely left the bridge, it is possible to use the strain measurements in free vibration to extract the 1st natural frequency of the bridge. This was found to be 3.6 Hz. This, coupled with the scanning frequency of 512 Hz used to obtain the measurements, governed the number of points to be used in the MAF used to remove the bridge dynamic component (Section 2.2.2). Figure 20 shows the filtered strains, again for the 2-axle truck travelling at 28.4 km/hr.

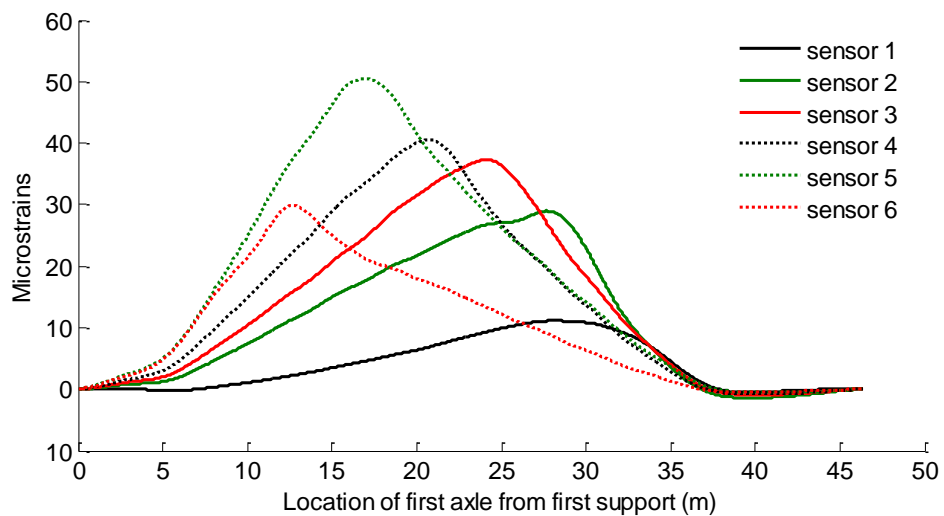


Figure 20. Filtered strains for the 2-axle truck travelling at 28.4 km/hr.

Although there are multiple runs of two trucks available (at different velocities) to calibrate the system, a higher number of runs would have been desirable (e.g., 20 for the sample in Figure 12). Figure 21 shows the influence line calculated for the mid-span location, (location 4, representative of all six) along with the influence lines calculated using the individual events to show the variation obtained using each single event.

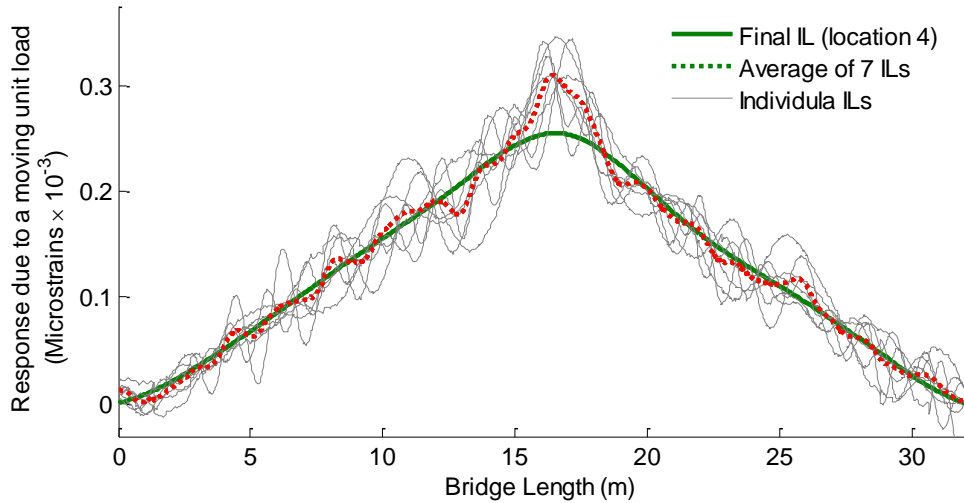


Figure 21. Influence line calculated for lane 2, location 4.

Figure 22 shows the final influence lines calculated for all six locations. These influence lines are again for lane 2. The influence lines presented in Figure 22 are not the exact influence lines of the bridge, but an approximation given the available experimental data.

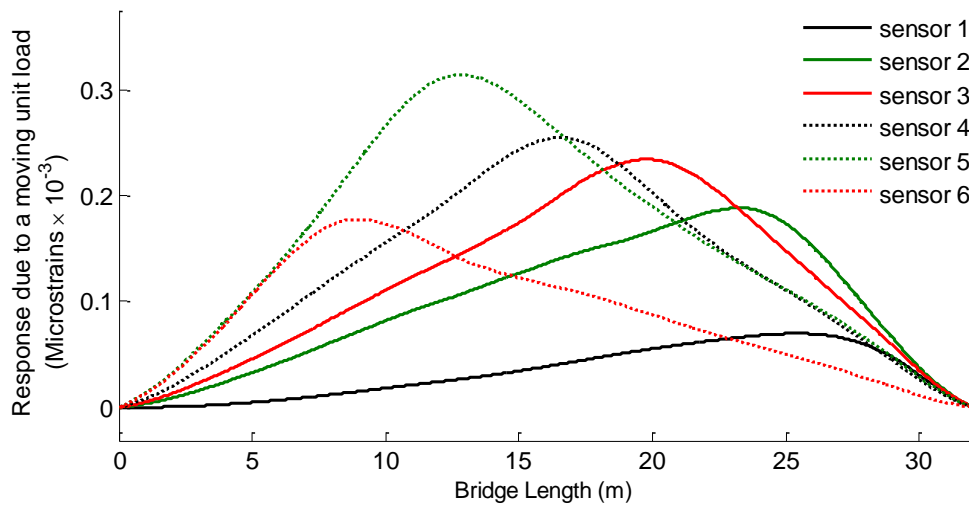


Figure 22. Influence lines calculated for all six locations of lane 2.

3.2 Experimental Results

To show an example of the force history predictions attained using the algorithm, Figure 23 is presented. It shows the predictions for the case of the 2-axle truck crossing lane 2 at 59.95 km/hr.

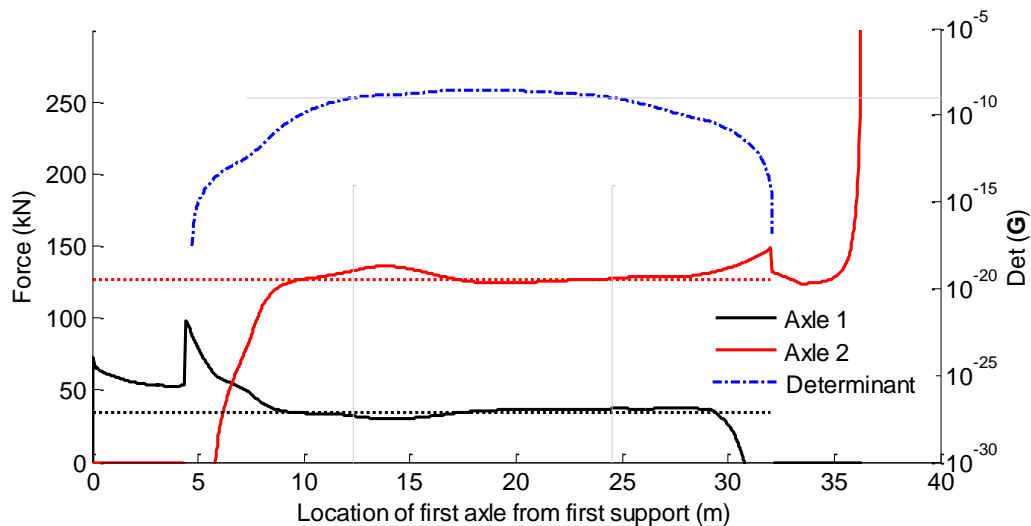


Figure 23. Force predictions for the 2-axle travelling in lane 2 at 59.95 km/hr.

The actual static axle weights are plotted dotted in the figure and the force history predictions plotted with solid lines. The secondary right-hand y-axis refers to $\det(\mathbf{G})$ which is plotted with dash-dot line-type. The predictions shown in Figure 23 are, for the most part, very accurate. Peaks can be noticed in the first axle prediction as the second axle enters the bridge and in the second axle prediction as the first axle leaves the bridge. In choosing the limits of the force predictions to be used in calculating the axle weights the limit of determinant is set to 1×10^{-9} . The resulting errors in the predicted axle weights are 2.2% and 1.7% for the first and second axles respectively (the error in GVW is 1.8%).

The influence line for mid-span location is used to test Moses' algorithm. The percentage errors of the axle weights calculated are -0.5% and 2.9% for the first and second axles respectively (GVW error is 2.2%). Both algorithms perform well in this case, with the proposed multiple sensor algorithm being slightly better.

In the case of the 3-axle truck, the rear tandem is treated as a single unknown for both algorithms. Figure 24 shows the predictions the 3-axle truck travelling in lane 2 at 56.80 km/hr.

The predictions in this case are more erratic, particular in the zones of transition from axles entering/exiting the bridge. Using the determinant as an indicator of the levels of confidence that can be expected works well here, removing those most erratic portions of the predictions from the final calculation of axle weights.

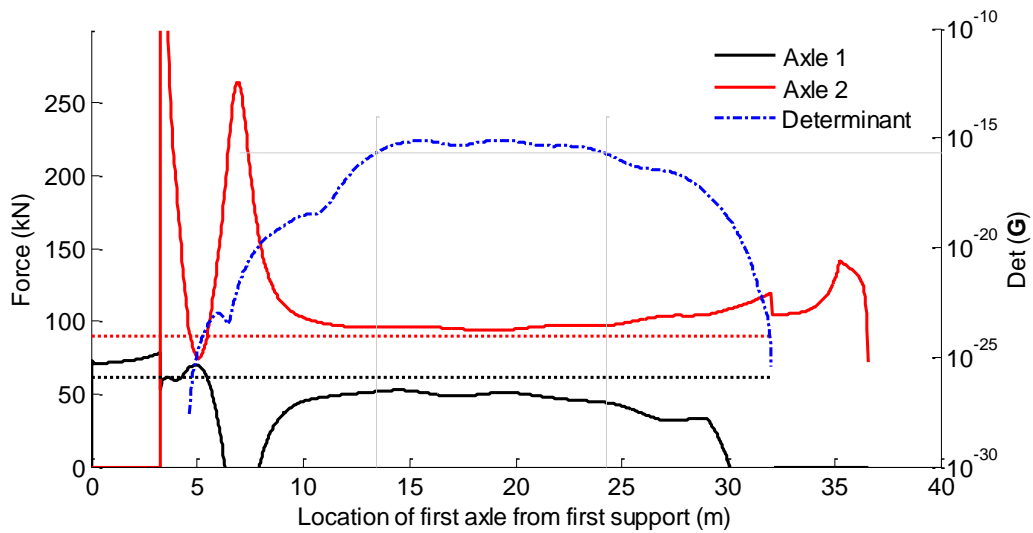


Figure 24. Force predictions for the 3-axle travelling in lane 2 at 56.80 km/hr.

Figure 24 highlights other valuable feature of the proposed algorithm, that is, the ability to spot potentially erroneous predictions. In this case, the portion of the predictions intended to be used to calculate the axle weights (indicated as between the light vertical bound lines) is not horizontal, particularly in the case of the axle 1 predictions. As the axle spacings are known to be exact, this is likely a case of the velocity having been misread, or that the truck accelerated or decelerated ever so slightly while traversing the bridge. As in this case the actual axle weights are known, it is possible to apply an optimisation procedure to the problem to optimise for a velocity that minimises the errors in axle weights. The results of this optimisation procedure are shown in Figure 25. The optimum velocity was found to be 56.16 km/hr.

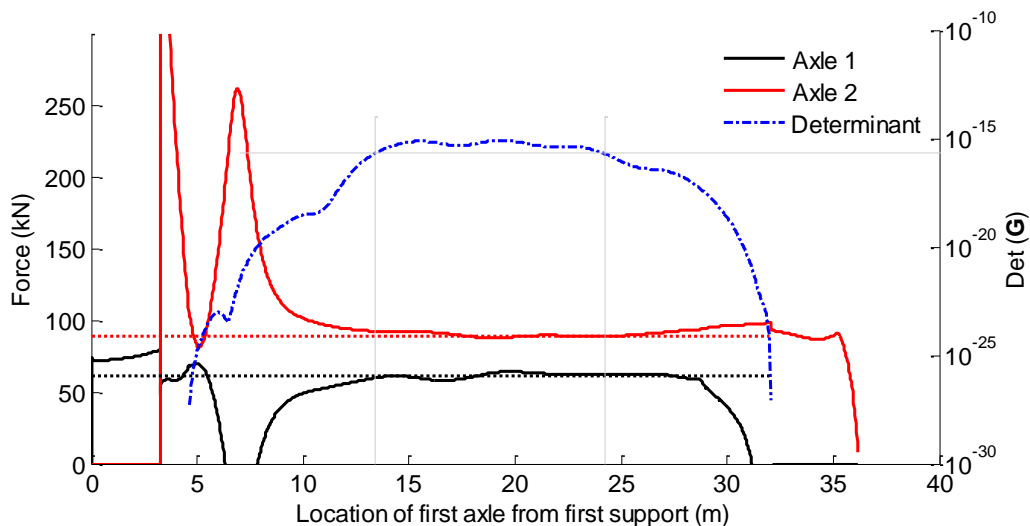


Figure 25. Force predictions for the 3-axle travelling in lane 2 using the corrected velocity of 56.16 km/hr.

The velocity found to minimise the errors in axle weights was 0.989×56.80 km/hr, a velocity very close to that which gave Figure 24. As the force history predictions between the vertical

bound lines have flattened, this supports the theory that a slight inaccuracy in the reading of velocity is the cause of the error. The percentage errors in the predictions of the first axle and an axle of the rear tandem are 0.4% and 0.4% respectively (GVW error is 0.4%). In contrast, errors by Moses' algorithm, including the correction of the misread velocity value, are, -21.7% and 9.4% for the first and second axles respectively (GVW error is 1.5%).

Figure 26 presents the results of the entire data set of seventeen runs. The x-axis provides a run number. Runs 1-4 represent the 2-axle truck in lane 1; runs 5-7 represent the 2-axle truck in lane 2; runs 8-13 represent the 3-axle truck in lane 1; runs 14-17 represent the 3-axle truck in lane 2. The drivers of the trucks were instructed to aim for velocities of 15 km/hr, 30 km/hr and 60 km/hr, hence the velocities of each of the runs is roughly one of these values.

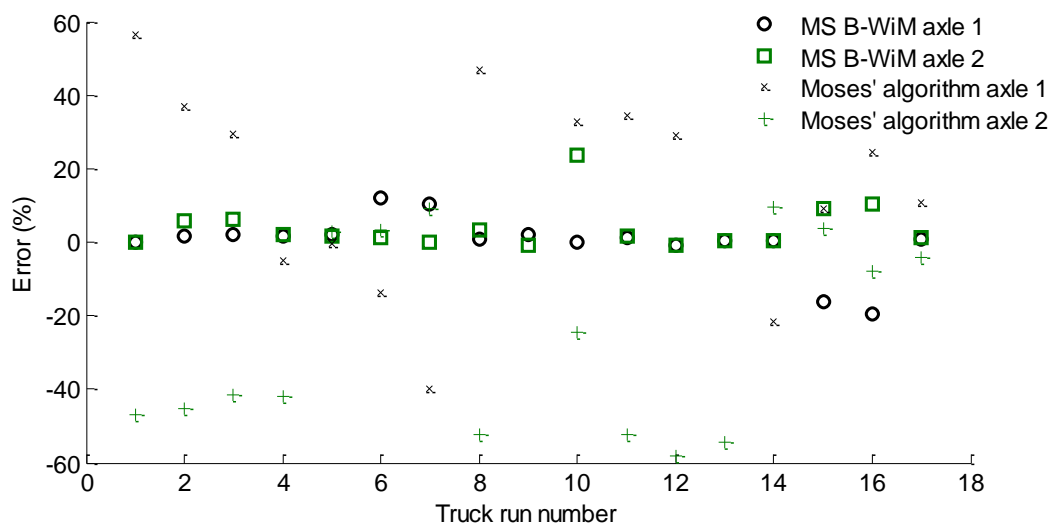


Figure 26. Errors for all seventeen runs.

The results of those runs in lane 1 were worse than those in lane 2 for both the 2-axle and 3-axle trucks. The results presented use velocities calculated in the optimisation procedure described above. The corrected velocities were very close to those which the system recorded in each case, with the average adjustment being 1.69%.

The errors of Moses' algorithm are quite substantial in some cases. This is due, at least in part, to the high levels of dynamics present in the measured responses. Mean errors of 15.3% and -23.6% are obtained using Moses' algorithm for the first and second axles respectively (mean GVW error is 15.3%), while for the proposed algorithm, mean errors of -0.1% and 3.9% are obtained for first and second axles respectively (mean GVW error is 0.7%).

4. Conclusions

A novel Bridge WIM algorithm utilising strain sensors at multiple longitudinal locations has been presented. The algorithm outputs a force prediction for each axle of the vehicle at each

point in time that bridge measurements are taken. Studying the determinant of the matrix of the system equations allows those portions of the force history predictions, which are most ill-conditioned, and hence erroneous, to be identified. Accordingly, those instants at which the system equations become detrimental to an accurate prediction have not been used in the calculations of static axle weight, resulting in increased accuracy of the inferred axle weights. The effects of a falsely measured vehicle velocity or axle spacing have been discussed. The number of vehicles required to calibrate the system have been examined, as well as the method of indentifying the bounds of the more accurate portions of the force history predictions. The proposed algorithm has also been verified with experimental measurements from a beam-and-slab bridge in Slovenia. Both numerical simulations and experimental data have shown that the algorithm improves predictions over current Bridge WIM algorithms.

5. References

- [1] ARCHES program, Assessment and rehabilitation of central European Highway Structures. *WP2: Structural Assessment and Monitoring*, EU 6th Framework, 2006-2009, 2009. Available at: <http://arches.fehrl.org/> (Accessed 17th December 2010).
- [2] Brady SP, OBrien EJ., Znidarič A. The Effect of Vehicle Velocity on the Dynamic Amplification of a Vehicle crossing a Simply Supported Bridge. *ASCE, Journal of Bridge Engineering*, 2006;11(2):241-249.
- [3] Cantero D, González A, OBrien EJ, Comparison of bridge dynamic amplification due to articulated 5-axle trucks and large cranes. *Baltic Journal of Road and Bridge Engineering* 2011;6(1):39-47.
- [4] Cebon D, Newland DE. Artificial generation of road surface topography by the inverse F.F.T. method. *Vehicle System Dynamics*, 1983;12(1):160-165.
- [5] Cebon D. Interaction between heavy vehicles and roads. *Society of Automotive Engineers*, SP-951, 1993.
- [6] Cebon D. *Handbook of Vehicle–Road Interaction*, Swets & Zeitlinger, 1999.
- [7] Chatterjee P, OBrien EJ, Li Y, González A. Wavelet domain analysis for identification of vehicle axles from bridge measurements. *Computers and Structures*, 2006;84:1792–1801.
- [8] COST 323. Weigh-In-Motion of Road Vehicles. In: Jacob B, OBrien EJ, Jehaes S, editors. Final report of the COST 323 action (WIM-LOAD), 1993_1998. LCPC. Paris; 2002.
- [9] Deesomsuk T, Pinkaew T. Effectiveness of Vehicle Weight Estimation from Bridge Weigh-in-Motion. *Advances in Civil Engineering*, vol. 2009, Article ID 312034, 13 pages, 2009. doi:10.1155/2009/312034.

- [10] Dempsey AT, Jacob B, Carracilli J. Orthotropic Bridge WIM for determining Axle and Gross Vehicle Weights. *Proceedings of the Final Symposium of the project WAVE*, Ed. B Jacob, 227-238. Hermes Science Publications: Paris, France, 1999.
- [11] El-Madany MM. Design optimization of truck suspensions using covariance analysis. *Computers & Structures*, 1988;28(2):241-246.
- [12] Fu TT, Cebon D. Analysis of a truck suspension database. *International Journal of Heavy Vehicle Systems* 2002;9(4):281–297.
- [13] Gillespie TD, McAdam CC, Hu GT, Bernard JE, Winkler CB. *Simulation of effects of increased truck size and weight*. University of Michigan, Highway Safety Research Institute, 1979.
- [14] González A, Rowley C, OBrien, EJ. A general solution to the identification of moving vehicle forces on a bridge. *International Journal of Numerical Methods in Engineering*, 2008;75(3):335-354.
- [15] Gonzalez, A. (2010) 'Vehicle-bridge dynamic interaction using finite element modelling' In: David Moratal (eds). *Finite Element Analysis*. Croatia: Sciyo, pp. 637-662.
- [16] Green MF, Cebon D, Cole DJ. Effects of vehicle suspension design on dynamics of highway bridges. *ASCE Structural Engineering*, 1995;121(2):272-282.
- [17] Hansen PC. Analysis of discrete ill-posed problems by means of the L-curve. *SIAM Review*, 1992;34(4):561-580.
- [18] Harris NK, OBrien EJ, González A. Reduction of bridge dynamic amplification through adjustment of vehicle suspension damping. *Journal of Sound and Vibration*, 2007;302(3):471-485.
- [19] International Organization for Standardization ISO. *Mechanical vibration – Road surface profiles - Reporting of measure data, ISO8608 (BS7853:1996)*, 1995.
- [20] Kenyon CH. Practical on-board weigh in-motion system for commercial vehicles. *Proceedings - Spie the International Society for Optical Engineering*, 1996;2903(16):156-163.
- [21] Kim HJ, Choi K, Lee HB, Jung HK, Hahn SY. A New Algorithm for Solving Ill-Conditioned Linear Systems. *IEEE transactions on Magnetics*. 1996;32(3):1373-1376.
- [22] Kirkegaard PH, Nielsen SRK, Enevoldsen I. Heavy vehicles on minor highway bridges—dynamic modelling of vehicles and bridges, Report in Department of Building Technology and Structural Engineering, Aalborg University, ISSN1395-7953R9721, 1997.

- [23] Law SS, Fang YL. Moving force identification: optimal state estimation approach. *Journal of Sound and Vibration*, 2001;239(2):233-254.
- [24] Matlab. The MathWorks, Inc., MATLAB, Version 6: USA, 2003. <http://www.mathworks.com> (Accessed 17th December 2010).
- [25] McNulty P, OBrien EJ. Testing of a bridge weigh-in-motion system in cold environmental conditions. *ASME Journal of Evaluation and Testing*, 2003;105:233-249.
- [26] Moses F. Weigh-In-Motion System using Instrumented Bridges. *ASCE Journal of Transportation Engineering*, 1979;105(3):233-249.
- [27] OBrien EJ, Quilligan M, Karoumi R. Calculating an Influence Line from Direct Measurements. *Proceedings of the Institution of Civil Engineers: Bridge Engineering*, 2006;159(BEI):31-34.
- [28] OBrien EJ, Rowley CW, González A, Green MF. A regularised solution to the Bridge Weigh-in-Motion equations. *International Journal of Heavy Vehicle Systems* 2009;16(3):310–327.
- [29] Peters RJ. An Unmanned and Undetectable Highway Speed Vehicle Weighing System. *Proceedings 13th ARRB Conference*, 1986;13(6):70-83.
- [30] Rowley CW, OBrien EJ, González A, Žnidarič A. Experimental testing of a moving force identification bridge weigh-in-motion algorithm. *Experimental Mechanics* 2009;49(5):743–746.
- [31] Sivakumar B, Ghosn M, Moses F. Protocols for Collecting and Using Traffic Data in Bridge Design. NCHRP web-only document 135. Transportation Research Board, National Research Council: Washington, DC, 2008.
- [32] Snyder RE. Field Trials of Low-Cost Bridge WIM. *Publication FHWA-SA-92-014*: Washington DC, 1992.
- [33] Tedesco JW, McDougal WG, Ross CA. *Structural Dynamics, Theory and Applications*, Addison-Wesley, 1999.
- [34] Tikhonov AN, Arsenin VY. *Solutions of ill-posed problems*, New York: John Wiley & sons, 1977.
- [35] Wang TL, Huang D. *Computer modelling analysis in bridge evaluation*. Florida International University, Highway planning and Research Program, 1992.
- [36] WAVE. Weighing-in-motion of Axles and Vehicles for Europe, Report of Work Package 1.2. Eds. O'Brien, E.J., & A., Žnidarič, A., Ljubljana, Slovenia. 2001.
- [37] Wong JY, *Theory of Ground Vehicles*, Wiley: NewYork, 1993.

- [38] Xue XJ, Kozaczek KJ, Kurtz SK, Kurtz DS. A Direct Algorithm for Solving Ill-Conditioned Linear Algebraic Systems. *Advances in X-ray Analysis*, 2000;42:629-633.
- [39] Yang B. *Stress, strain and structural dynamics*. Elsevier Academic Press, 2005.
- [40] Žnidarič A, Baumgärtner W. Bridge Weigh-In-Motion Systems – An Overview. *Pre-proceedings of the 2nd European Conference on Weigh-In-Motion*, eds. EJ OBrien and B Jacob, 139-152. Lisbon, Portugal, 1998.
- [41] Žnidarič A, Dempsey A, Lavrič I, Baumgärtner W. Bridge WIM Systems without Axle Detectors. *Proceedings of the Final Symposium of the project WAVE*, Ed. B Jacob, 101-110. Hermes Science Publications: Paris, France, 1999a.
- [42] Žnidarič A, Lavrič I, Kalin J. Bridge WIM Measurements on Short Slab Bridges. *Proceedings of the Final Symposium of the project WAVE*, Ed. B Jacob, 217-226. Hermes Science Publications: Paris, France, 1999b.
- [43] Žnidarič A, Lavrič I, Kalin J. (2002), “The Next Generation of Bridge Weigh-in-Motion Systems”, in *Proceedings of the 3rd International Weigh-in-Motion Conference*, Orlando.